Two-Phase Modeling of DDT in Granular Materials: Reduced Equations

A. K. Kapila
Rensselaer Polytechnic Institute, Troy, New York

R. Menikoff, J. B. Bdzil, S. F. Son
Los Alamos National Laboratory, Los Alamos, New Mexico

and

D. S. Stewart, University of Illinois, Urbana, Illinois

October 10, 2000

Abstract

Of the two-phase mixture models used to study the deflagration-to-detonation transition in granular explosives, the Baer-Nunziato (BN) model is the most highly developed. It allows for unequal phase velocities and phase pressures, and includes source terms for drag and compaction that strive to erase velocity and pressure disequilibria respectively. Since typical time scales associated with the equilibrating processes are small, source terms are stiff. This stiffness motivates the present work where we derive two reduced models in sequence, one with a single velocity and the other with both a single velocity and a single pressure. These reductions constitute outer solutions in the sense of matched asymptotic expansions, with the corresponding inner layers being just the partly dispersed shocks of the full model. The reduced models are hyperbolic and are mechanically as well as thermodynamically consistent with the parent model. However, they cannot be expressed in conservation form and hence require a regularization in order to fully specify the jump conditions across shock waves. Analysis of the inner layers of the full model provides one such regularization [Kapila *et al.*, Phys. Fluids **9**, 3885 (1997)], although other choices are also possible. Dissipation associated with degrees of freedom that have been eliminated is restricted to the thin layers and is accounted for by the jump conditions.

PACS: 47.55.Kf, 83.10.Ff, 05.70.Ln, 83.50.Tq

1 Introduction

This paper is one of a sequence of articles on the modeling, analysis and numerical simulation of deflagration-to-detonation transition (DDT) in granular energetic materials. It has long been known that the combustion behavior of a homogeneous sample of a solid explosive differs markedly from that of a porous or granular sample. When subjected to a relatively mild stimulus, the latter shows an increased incidence of DDT, a sequence of events whereby an initially slow mode of burning accelerates into a violent, rapid mode. The recognition that porosity may increase in an explosive sample unintentionally, through degradation over time or through accidental damage, has lent some urgency to the need for improved, quantitative understanding of the manner in which porous, high-energy explosives burn. Here one seeks to develop the framework for a continuum-scale model for predicting the DDT behavior of porous explosives over a broad range of conditions. Such models are needed to describe accurately the response of engineered explosive systems with a continuum-level hydrodynamics code.

A natural approach is to treat the porous explosive as a two-phase mixture of interacting continua, consisting of grains of reacting solid and the gaseous products of combustion. This approach dates back to at least twenty five years ago, and is exemplified in the work of Baer and Nunziato (BN) [1]; their paper also contains an extensive historical review. Contemporaneous studies by Butler and Krier [2] and Butler [3], the earlier work of Gokhale and Krier [4], and the later papers of Powers, Stewart and Krier, [5], [6], also deserve mention. More recently, the present authors have re-examined the BN model comprehensively and critically, with an eye on its theoretical foundations, on the appropriateness of the modeling assumptions, and on the way in which experimental information is incorporated into the theory [7]. There we suggest certain modifications, which allow one to remove inconsistencies from the original formulation, especially those pertaining to single-phase limits of the model, and the apportioning of the work of compaction between the phases. Possible generalizations are identified as well.

A fundamental assumption underlying the two-phase description is that each phase is in local thermodynamic equilibrium. Nonequilibrium interactions do occur between the phases, driven by the processes of drag, compaction, heat transfer and chemical reaction. These processes are represented in the model by source terms that lead to the exchange of mass, momentum and energy across the interfaces separating the phases. The BN model is hyperbolic, and the presence of source terms causes solutions of the model to exhibit a complex wave structure.

Each nonequilibrium process has a characteristic rate, which determines the corresponding length and time scales for equilibration. Estimates reveal that the length scale for velocity equilibration is very small, causing the source terms associated with drag between the phases to be very stiff. Carrying two velocity variables, as BN does, is then an unnecessary encumbrance in substantial regions of the flow, since significant differences in velocity are confined to narrow velocity equilibration layers. However, the drag related momentum and energy exchange between the phases, required to support the equilibration of velocities, must be accounted for in a consistent fashion. As we show, the two velocities cannot simply be set equal to one another as is done in recent numerical work by Massoni *et al.* [8] and Saurel & Abgrall [9]. The product of a large drag coefficient and a small velocity difference resolves as an $O(1)$ exchange term even in smooth regions. Additionally, two velocities give rise to computational difficulties at interfaces between porous and nonporous materials, where the two velocities of the porous material must adjust to the single velocity of the nonporous material. These considerations suggest a systematic asymptotic reduction of the BN model to one that carries a single velocity, supplemented by appropriate jump conditions across thin zones in which $O(1)$ velocity differences equilibrate.

The length scale for pressure equilibration is found to be small as well, at pressures above the yield strength of the explosive. This suggests a further reduction to a nominally one-pressure, one-velocity description.

Two further reductions are possible, in principle. A single temperature would lead to the single

fluid reactive Euler equations, whereas chemical equilibrium would reduce the model further to just the Euler equations. However, estimates of the scales over which temperatures equilibrate imply that thermal equilibrium is not justified, nor is chemical equilibrium since chemical reaction takes place over rather broad regions of the flow field for the DDT problems of interest.

The purpose of this paper is to derive the reduced models and study aspects of their mathematical structure. The reductions are carried out sequentially, velocity equilibration followed by pressure equilibration, it being well-known that pressure equilibrium alone leads to equations of mixed hyperbolic-elliptic type which are inappropriate for describing evolutionary problems [10], [11]. The limits leading to the reduction are singular, in the sense of matched asymptotics. Therefore, the reductions constitute outer expansions, holding outside thin spatial regions (relaxation layers) and possibly thin temporal regions (initial layers).

We show that the reduced models are thermodynamically consistent. This is a consequence of each relaxation process in the full model being separately dissipative [7]. All the dissipation associated with the non-equilibrium degrees of freedom eliminated in the reductions occurs in the thin inner layers of the asymptotic expansion. These layers correspond to partly dispersed waves (shocks followed by thin relaxation layers). Viewed on the scale of the outer expansion, these thin layers are the shocks of the reduced model.

Recent work of Chen, Levermore and Liu [12] examines hyperbolic conservation laws with a certain class of stiff relaxation terms. These authors point out that in general, a formal equilibrium limit does not necessarily lead to a lower-order system that is hyperbolic, and even when it does, there still remains the question of whether the reduced system is an attractor, and hence a suitable approximate representation of the dynamics of the full system. It is further shown [12] that the reduced system is stable if it satisfies the so-called subcharacteristic condition, *i.e.*, if its characteristic speeds do not exceed (and in fact, interlace between) those of the full system. In a stable system the relaxation terms are dissipative; equivalently, the system is endowed with an appropriate entropy.

The source terms for the BN-model are not in the class considered in [12] and the reduced models derived here, though hyperbolic, are incapable of being fully expressed in a conservative form. However, there does exist an explicit entropy in our system, which allows the dissipative (and hence stable) nature of the reduction to be demonstrated. Additionally, the subcharacteristic condition is found to be satisfied as well.

A further consequence of the lack of conservation form is that the reduced systems do not possess a full complement of jump conditions across a spatial discontinuity, and must therefore be appropriately supplemented or regularized. The regularization may be obtained by extracting the needed information from structure analyses of the large-gradient relaxation zones. This corresponds to determining steady-state wave profiles of the underlying full model. Such an inner analysis for the pressure-equilibration zone, or compaction wave, is presented in this paper; the corresponding treatment of the velocity-relaxation zone was carried out in [13]. Alternatively the information could be garnered independently of the full BN model, by constructing subscale models of the physical processes within the discontinuities, based upon experiments and/or microscale computations. This is an important point since the continuum model tacitly averages over small scale material inhomogeneities and breaks down for relaxation layers that are thinner than the grain diameter. In effect, the grain diameter of a granular material plays a role analogous to the mean free path length of a molecule in gas dynamics.

Regularization of the reduced models corresponds to specifying the dissipation within a "shock profile." The non-uniqueness arises from the freedom one has to apportion the shock energy between the solid and the gas phases; a similar degree of freedom arose in our re-examination of the thermodynamic formulation of the BN model [7]. At the same time, regularization is not completely arbitrary; to be physical, the entropy of each phase is required to be non-decreasing. This is analogous to the dissipation inequality used to constrain the source terms in [7]. Further issues relating to regularization, and numerical implementation of the reduced models, are explored in a forthcoming paper [14].

2 The BN model

The two-phase BN model has evolved significantly since it was first introduced by Baer and Nunziato [1]. Some of the modifications are due to the original authors themselves, and these pertain principally (though not exclusively) to the treatment of the chemical reaction [15]; see also [16] for additional details. Others, intended to remove inconsistencies and improve and generalize the source terms are the result of our comprehensive review of the continuum-mechanical underpinnings of the model [7]. For the purposes of asymptotic reduction we consider a revised version of BN which, while not the most general, differs in three crucial ways from the original; it adds a compaction potential to the solid-phase internal energy, reapportions compaction work between the phases, and modifies the portion of the interphase energy exchange that is due to chemical reaction. The revised terms will be explicitly identified shortly, subsequent to the introduction of the governing equations. The latter constitute the following set of seven PDEs, representing mass, momentum and energy balance for each phase, and a compaction law:

Mass balance

$$\frac{\partial}{\partial t}\Big(\phi_s\rho_s\Big) + \frac{\partial}{\partial x}\Big(\phi_s\rho_s u_s\Big) = \mathcal{C}, \tag{1}$$

$$\frac{\partial}{\partial t}\Big(\phi_g\rho_g\Big) + \frac{\partial}{\partial x}\Big(\phi_g\rho_g u_g\Big) = -\mathcal{C}; \tag{2}$$

Momentum balance

$$\frac{\partial}{\partial t}\Big(\phi_s\rho_s u_s\Big) + \frac{\partial}{\partial x}\Big(\phi_s\rho_s u_s^2 + \phi_s P_s\Big) = P_g\frac{\partial\phi_s}{\partial x} + \tilde{\mathcal{M}}, \tag{3}$$

$$\frac{\partial}{\partial t}\Big(\phi_g\rho_g u_g\Big) + \frac{\partial}{\partial x}\Big(\phi_g\rho_g u_g^2 + \phi_g P_g\Big) = -P_g\frac{\partial\phi_s}{\partial x} - \tilde{\mathcal{M}}; \tag{4}$$

Energy balance

$$\frac{\partial}{\partial t}\Big[\phi_s\rho_s E_s\Big] + \frac{\partial}{\partial x}\Big[\phi_s u_s(\rho_s E_s + P_s)\Big] = -P_g\mathcal{F} + P_g u_s\frac{\partial\phi_s}{\partial x} + \tilde{\mathcal{E}}, \tag{5}$$

$$\frac{\partial}{\partial t}\Big[\phi_g\rho_g E_g\Big] + \frac{\partial}{\partial x}\Big[\phi_g u_g(\rho_g E_g + P_g)\Big] = P_g\mathcal{F} - P_g u_s\frac{\partial\phi_s}{\partial x} - \tilde{\mathcal{E}}, \tag{6}$$

Compaction dynamics

$$\frac{\partial\rho_s}{\partial t} + \frac{\partial}{\partial x}\Big(\rho_s u_s\Big) = -\frac{\rho_s}{\phi_s}\mathcal{F}\,. \tag{7}$$

Here the subscripts s and g refer to the solid and the gas phase, respectively. The state variables for the phases are

$\rho_s,\ \rho_g$ = densities,
$V_s,\ V_g$ = specific volumes,
$e_s,\ e_g$ = specific internal energies,
$P_s,\ P_g$ = pressures,
$T_s,\ T_g$ = temperatures,
$\eta_s,\ \eta_g$ = specific entropies,
$u_s,\ u_g$ = particle velocities,
$\phi_s,\ \phi_g$ = volume fractions, subject to the saturation constraint $\phi_s + \phi_g = 1$.

In addition, $E_g = e_g + \frac{1}{2}u_g^2$ is the total gas specific energy, $E_s = e_s + \frac{1}{2}u_s^2$ is the total solid specific energy, and $e_s = e_{sp} + B$ where e_{sp} is the internal energy of the pure solid and $B(\phi_s)$ is the compaction

potential energy. Equations of state are required for each constituent. These are generally of the form

$$P_a = P_a(\rho_a, e'_a), \qquad T_a = T_a(\rho_a, e'_a),$$

where $e'_g = e_g$ and $e'_s = e_{sp}$. Inclusion of the compaction potential in the solid internal energy represents the first of the three modifications referred to above.* We assume that each isolated phase satisfies the thermodynamic relation†

$$de'_a = -P_a dV_a + T_a d\eta_a. \tag{8}$$

In addition, we take $B(\phi_s)$ to be strictly increasing and convex, *i.e.*, $dB/d\phi_s > 0$ and $d^2B/d\phi_s^2 > 0$. Consequently, the intragranular stress or configuration pressure defined by

$$\beta_s(\phi_s, \rho_s) = \rho_s \phi_s \frac{dB(\phi_s)}{d\phi_s} \tag{9}$$

is positive and monotonically increasing as ϕ_s increases. We note that β_s depends on both ϕ_s and ρ_s, rather than only on ϕ_s as in the original BN-model [1]. This dependence is motivated by the approximation used for the mixture free energy discussed in [7].

Source terms representing interaction between the phases appear on the right-hand sides of the balance equations. In the mass conservation equation the source $\mathcal{C}$ represents the rate at which gas is converted into solid. Consequently, $\mathcal{C} < 0$ when the solid burns. The precise expression for $\mathcal{C}$ depends upon the particulars of the kinetics and will not be needed in our discussion. Source terms proportional to $\partial\phi_s/\partial x$, appearing in both the momentum and energy balance, are the so-called *nozzling terms*. These terms model momentum and energy exchange between the phases that arise as the result of an effective change in the cross-sectional area of a virtual stream tube in the gas phase, see [7]. The term proportional to $\mathcal{F}$ in the energy balance represents compaction work. We note that the coefficient of the compaction work term is P_g in contrast to $P_s - \beta_s$ in the original BN-model [1]. This is the second modification, justified in detail in [7].

Additional source terms are the compaction rate $\mathcal{F}$, the residual momentum exchange $\tilde{\mathcal{M}}$ due to burning and drag, and the residual energy exchange $\tilde{\mathcal{E}}$ associated with burning, drag and heat transfer. We assume these sources have the form

$$\mathcal{F} = \phi_s \phi_g (P_s - P_g - \beta_s)/\mu_c, \tag{10}$$

$$\tilde{\mathcal{M}} = \mathcal{C}\, u_s + (\delta + \frac{1}{2}\mathcal{C})(u_g - u_s)\,, \tag{11}$$

$$\tilde{\mathcal{E}} = (E_s + \beta_s V_s)\,\mathcal{C} + \left(\delta + \tfrac{1}{2}\,\mathcal{C}\right)(u_g - u_s)\,u_s + (T_g - T_s)\mathcal{H}\,, \tag{12}$$

where δ is the drag coefficient, $\mathcal{H}$ the heat-transfer coefficient, and μ_c the compaction viscosity. Except for the $\beta_s V_s \mathcal{C}$ term in $\tilde{\mathcal{E}}$, these are the same expressions used in the original BN-model [1]. This modification, the last in the list of three, represents a slight departure from the derivation in [7]. It remains in agreement with the dissipation inequality, and the reason for its introduction will be apparent following the appearance of the entropy production equations below.

The PDEs have characteristic speeds [1, 18, 7]

$$u_s,\ u_s,\ u_g,\ u_s \pm c_s,\ u_g \pm c_g\ ,$$

*Typically, B is small and may be neglected. It is however needed within the present formulation of the model for thermodynamic consistency and to guarantee that the entropy inequality is satisfied [7]. The model can be extended in a thermodynamically consistent fashion in order that quasi-static compaction is dissipative and irreversible [17].

†The solid phase specific energy (internal + compaction potential) satisfies the relation given in the original derivation of the BN-model [1], $de_s = de_{sp} + dB = -P_s dV_s + T_s d\eta_s + \frac{\beta_s}{\phi_s \rho_s} d\phi_s$, where β_s is defined by (9).

where the pure phase sound speeds are, as usual, determined by

$$c_a^2 = \left.\frac{\partial P_a}{\partial \rho_a}\right|_{\eta_a} .$$

The model is hyperbolic except when $u_s = u_g \pm c_g$ [18]. In practice the drag coefficient is sufficiently large such that $|u_s - u_g| < c_g$ and the restricted set on which the model is degenerate does not cause any difficulty. Though the nozzling terms are not in conservation form they don't affect the wave structure, provided that ϕ_s is initially continuous, since it follows from Eqs. (1) and (7) that the volume fraction is continuous across a shock.

2.1 Equations in alternate form

There are other forms in which the governing equations can be written. First, the compaction equation, Eq. (7), with the aid of the solid-phase mass balance equation, Eq. (1), can be rewritten as a rate equation for the evolution of ϕ_s,

$$\frac{\partial \phi_s}{\partial t} + u_s \frac{\partial \phi_s}{\partial x} = \mathcal{F} + \frac{\mathcal{C}}{\rho_s}. \tag{13}$$

Second, the total energy balance for each phase may be replaced by the internal-energy balance, obtained by removing the kinetic component from the phase-specific total energy by using the appropriate mass and momentum equations.

Solid internal-energy balance

$$\frac{\partial}{\partial t}\Big(\phi_s \rho_s e_{sp}\Big) + \frac{\partial}{\partial x}\Big(\phi_s \rho_s u_s e_{sp}\Big) + \phi_s P_s \frac{\partial u_s}{\partial x} = e_{sp}\,\mathcal{C} - (T_s - T_g)\mathcal{H} - (P_g + \beta_s)\mathcal{F}. \tag{14}$$

Gas internal-energy balance

$$\begin{aligned}\frac{\partial}{\partial t}\Big(\phi_g \rho_g e_g\Big) + \frac{\partial}{\partial x}\Big(\phi_g \rho_g u_g e_g\Big) + \phi_g P_g \frac{\partial u_g}{\partial x} = &-(e_s + \beta_s V_s)\,\mathcal{C} + (T_s - T_g)\mathcal{H} + P_g \mathcal{F} \\ &+ \left[P_g (u_g - u_s)\frac{\partial \phi_s}{\partial x} + \delta (u_s - u_g)^2\right].\end{aligned} \tag{15}$$

Application of the thermodynamic relation, Eq. (8), and the mass equations (2) leads to the entropy equations,

Solid dissipation rate

$$\phi_s \rho_s T_s \Big(\frac{\partial}{\partial t} + u_s \frac{\partial}{\partial x}\Big)\eta_s = \frac{\phi_s \phi_g}{\mu_c}(P_s - P_g - \beta_s)^2 - (T_s - T_g)\mathcal{H}\ , \tag{16}$$

Gas dissipation rate

$$\phi_g \rho_g T_g \Big(\frac{\partial}{\partial t} + u_g \frac{\partial}{\partial x}\Big)\eta_g = \delta (u_s - u_g)^2 + (T_s - T_g)\mathcal{H} - \big[H_s - H_g - (P_s - P_g - \beta_s)V_s\big]\mathcal{C}\ , \tag{17}$$

where $H_s = e_s + P_s V_s$ and $H_g = e_g + P_g V_g$ are the solid and gas enthalpies, respectively. We note that all the dissipation from compaction is apportioned to the solid, and all the dissipation from drag and burning to the gas. Had we not included the $\beta_s V_s \mathcal{C}$ term in $\tilde{\mathcal{E}}$, the portion $\beta_s V_s \mathcal{C}$ of the compaction energy associated with burning would have been transferred, unnaturally in our view, from the gas to the solid.

The entropy inequality for the mixture is given by

$$\phi_s\rho_s\Big(\frac{\partial}{\partial t}+u_s\frac{\partial}{\partial x}\Big)\eta_s+\phi_g\rho_g\Big(\frac{\partial}{\partial t}+u_g\frac{\partial}{\partial x}\Big)\eta_g+(\eta_s-\eta_g)\mathcal{C}\geq 0\,. \tag{18}$$

The term in the overall entropy inequality proportional to $\mathcal{C}$ places a constraint on the reaction; see the discussion in [7]. For an irreversible reaction, $\mathcal{C}\leq 0$, this constraint can be expressed as

$$G_s-G_g\geq(T_g-T_s)\eta_s+(P_s-P_g-\beta_s)V_s\,, \tag{19}$$

where $G_a=H_a-T_a\eta_a$ is the Gibbs free energy. In mechanical and thermal equilibrium this reduces to the standard condition that the Gibbs free energy is a minimum, *i.e.,* $G_g<G_s$. Out of equilibrium there are correction terms proportional to the degree of thermal disequilibrium (T_g-T_s) and the degree of mechanical disequilibrium $(P_s-P_g-\beta_s)$. The natural and simple form of equation (19) is again a consequence of including the $\beta_sV_s\mathcal{C}$ term in the energy source $\tilde{\mathcal{E}}$; otherwise, η_s in equation (19) is replaced by $\eta_s-\beta_sV_s/T_s$, corresponding to the choice $\nu=1$ in [7].

Third, the BN equations are written above in a phase-specific form. It is convenient, and useful, to rewrite them in a form that is appropriate for the mixture. This is done by simply adding the corresponding single-phase balance equations. The results can be expressed in a form that also includes certain mixture variables. The latter are constructed by volume-weighted or mass-weighted averages of the phase-specific quantities, and are defined as follows.

$$\text{mixture density } \rho=\phi_s\rho_s+\phi_g\rho_g, \tag{20}$$
$$\text{mixture velocity } u=\lambda_su_s+\lambda_gu_g, \tag{21}$$
$$\text{mixture pressure } P=\phi_sP_s+\phi_gP_g, \tag{22}$$
$$\text{mixture internal energy } e=\lambda_s(e_{sp}+B)+\lambda_ge_g, \tag{23}$$
$$\text{mixture specific entropy } \eta=\lambda_s\eta_s+\lambda_g\eta_g, \tag{24}$$

where $\lambda_a=\phi_a\rho_a/\rho$ is the mass fraction of phases a. The mixture equations are given below.

Mixture mass balance

$$\frac{\partial\rho}{\partial t}+\frac{\partial}{\partial x}\Big(\rho u\Big)=0, \tag{25}$$

Mixture momentum balance

$$\frac{\partial}{\partial t}\Big(\rho u\Big)+\frac{\partial}{\partial x}\Big[P+\rho u^2+\frac{\phi_s\rho_s\phi_g\rho_g}{\rho}(u_s-u_g)^2\Big]=0, \tag{26}$$

Mixture energy balance

$$\begin{aligned}\frac{\partial}{\partial t}\Big[\rho\Big(e+\tfrac{1}{2}u^2\Big)+\frac{\phi_s\rho_s\phi_g\rho_g}{2\rho}(u_s-u_g)^2\Big]+\frac{\partial}{\partial x}\Big[\rho u\Big(e+\tfrac{1}{2}u^2\Big)+Pu+\Big(\frac{\phi_s\rho_s\phi_g\rho_g}{\rho}\Big)\Big(H_s-H_g\Big)(u_s-u_g)\\ +\frac{3u}{2}\Big(\frac{\phi_s\rho_s\phi_g\rho_g}{\rho}\Big)(u_s-u_g)^2+\frac{\phi_g\rho_g-\phi_s\rho_s}{2\rho}\Big(\frac{\phi_s\rho_s\phi_g\rho_g}{\rho}\Big)(u_s-u_g)^3\Big]=0.\end{aligned} \tag{27}$$

Any set of seven independent equations can be taken to be the governing set, and in what follows, we shall make a variety of choices based on convenience.

3 Length & Time Scales for Equilibration

The hyperbolic nature of the model guarantees that its transient solutions will feature waves and interactions among them. Typically the passage of a wavehead, such as a noncompacting shock,

over a quiescent bed initially at thermodynamic equilibrium will cause the two phases to be brought to different states of velocity, pressure and temperature behind the wavehead. Processes of drag, compaction and heat transfer will attempt to erase these differences and edge the phases towards equilibrium. Thus, waveheads will be followed by zones of relaxation whose length scales depend upon the magnitudes of the coefficients characterizing the relaxation processes: drag coefficient δ for velocity equilibration, compaction viscosity μ_c for pressure equilibration and heat transfer coefficient $\mathcal{H}$ for attainment of thermal equilibrium. For applications to the DDT tube tests [19, 20] we have in mind, we now provide estimates of the coefficients and the associated relaxation lengths, as motivation for the reduced models derived in later sections.

3.1 Velocity-equilibration scales

Relaxation of velocity differences is driven by drag, on a characteristic time that depends on the magnitude of the difference and the size of the drag coefficient. Many measurements of the drag coefficient have been made as a function of porosity, grain size, grain shape and material, though usually for relatively small imposed pressure differences across the bed. The key elements of the problem are displayed in the gas momentum equation without burn in Eq. (4),

$$(\phi_g \, \rho_g \,) \frac{du_g}{dt} + \phi_g \frac{\partial P_g}{\partial x} = -\delta \cdot u_g \ ,$$

where for simplicity, motion of the solid bed is neglected. Most of the measurements were performed under quasistatic conditions, so that the inertial terms, du_g/dt, are negligible and the force balance reduces to Darcy's law

$$\phi_g \frac{\partial P_g}{\partial x} = -\delta \cdot u_g \ .$$

Here the drag coefficient is $\delta = \mu_g/k$, with μ_g the dynamic viscosity of the gas and k the permeability of the porous solid.

In experiments carried out on granular HMX with 30 to 50 μm grains, Shepherd and Begeal [21] determined that permeability decreases from $k \approx 10^{-9}\,\mathrm{cm}^2$ at $\phi_g = 0.2$ to $k \approx 10^{-13}\,\mathrm{cm}^2$ at $\phi_g = 0.05$. The permeating gas was Nitrogen at room temperature and the driving pressures ranged from 0.69 to 138 MPa. More recently, Asay, Son and Bdzil [22] have extended the driving pressure range to 500 MPa and temperature to 4000 K. To prevent both compaction and reaction at these conditions, a silicon carbide (SiC) bed at $\phi_s = 0.74$ was used. These experiments show that drag is at least as big under these higher-pressure conditions as that measured by Shepherd and Begeal. When measured over a macroscopic length scale of a few cm, the gas permeation velocity was no more than 5 m/s, essentially insignificant when compared with that of high-speed combustion waves, observed to travel at $\approx 1000\,\mathrm{m/s}$ in $\phi_s = 0.74$ beds of HMX. Thus, these experiments showed that permeation over macroscale distances is measured in milliseconds in such beds and not the microsecond time scale associated with ignition and transition to detonation in DDT tube tests.

These permeabilities lead to a drag coefficient $\delta \approx 200\,\mathrm{kg}/(\mathrm{m}^3 \cdot \mu\mathrm{s})$. We now ask, with a drag coefficient this large, how long it takes for a preexisting $O(1)$ difference in the gas and solid velocity to relax. Assuming that the pressure changes over an $O(1)$ spatial scale, while the time scales like $1/\delta$, the leading terms in the gas momentum equation are

$$\phi_g \rho_g \frac{du_g}{dt_g} \sim -\ \delta \cdot u_g \ ,$$

yielding, for $\phi_g \rho_g \approx 10\,\mathrm{kg/m}^3$, a time constant for velocity equilibration of the order of

$$\tau_u \sim \phi_g \rho_g / \delta = 0.1\,\mu\mathrm{s} \ .$$

The corresponding length scale is $D\tau_u$ where the wave speed D is of the order of the solid sound speed, $c_s = 3\,\mathrm{mm}/\mu\mathrm{s}$. This leads to the estimate $\tau_u c_s \sim 0.3\,\mathrm{mm}$ for the velocity-equilibration length scale.

Typically, the grain size is about $100\,\mu$m or $0.1\,$mm. Therefore the relaxation length scale is of the order of the grain size. Physically this is quite reasonable; since the grains touch each other, there is no line-of-sight path through the granular bed and the resulting gas flow will be highly tortuous. This observation can be interpreted as saying that the mean free path of the gas phase relative to the solid phase is of the order of the grain size. The cell size for numerical simulations reported in the literature has almost always been greater than the grain size. In a subsequent paper [14], numerical experiments with the same empirical value of the drag coefficient as used in [1] will be presented, showing that the solid and gas velocities are nearly equal except for a narrow region about the shock front. This implies that the source terms for velocity equilibration are very stiff.

Drag can only become small after burning reduces the grain size resulting in much smaller grains suspended in the combustion products. By then the burn rate is usually sufficiently large so that the remainder of the solid is fully burnt in a short time. In this situation, drag plays a negligible role in the flow, compared to combustion.

In conclusion, analytic estimates of drag, numerical experiments on the BN-model, and permeation experiments, all show the velocity-relaxation length to be very small, so that one is led naturally to consider a reduced model with a single velocity field. To be sure, permeation on the scale of a few grains can be significant for short range transport of heat, and can affect the speed of combustion waves. However, the drag source term currently used in two phase models is appropriate for permeation over macroscopic length scales and slow time scales. In order to account for heat transport due to permeation on the mesoscale of a grain, a subscale drag model is needed, whether one employs a reduced model or not.

3.2 Pressure-equilibration scales

Pressure disequilibration is associated with dynamic compaction. To estimate the relevant scales, consider the porous bed compacting in the absence of gas. In this simplified case the BN compaction law, Eq. (13), reduces to

$$\frac{d\phi_s}{dt} = \frac{\phi_s \phi_g}{\mu_c}\Big(P_s - \beta_s\Big)\,, \qquad \text{with} \qquad P_s - \beta > 0\,, \tag{28}$$

where d/dt is now the convective derivative with respect to the solid velocity. This is an equation of relaxation type and yields the estimate

$$\tau_p \sim \frac{\mu_c}{P_s}$$

for the characteristic time for ϕ_s to adjust and the pressure to equilibrate to its equilibium value, $P_s = \beta_s(\phi_s, \rho_s)$.

Compaction profiles have been measured experimentally. For granular HMX with a mean grain size of $\sim 0.15\,$mm and $\phi_{s0} = 0.73$, representative values of the wave thickness Δx and rise time Δt are [23]: (i) $\Delta x = 0.4\,$mm and $\Delta t = 1\,\mu$s at $P_s = 1\,$kbar and (ii) $\Delta x = 0.2\,$mm and $\Delta t = 0.2\,\mu$s at $P_s = 7\,$kbar. These data are compatible with a compaction viscosity of $\mu_c = 0.2\,\mathrm{kbar}\cdot\mu\mathrm{s}$ [24], and reveal that the thickness of a compaction wave decreases with pressure, from about 3 to 1 grain diameters over the pressure range of interest. Consequently, in the absence of gas to resist compaction, the length scale for pressure equilibrium is a few grain diameters when the wave pressure is a few kbars.

For higher pressures, much greater than the solid yield strength, the grains deform plastically, and hence pressure differences between the phases cannot be supported, *i.e.,* the solid behaves like a fluid. Then the natural time constant for pressure equilibration would be determined by the

gas pore size and the transverse velocity at which the solid phase can expand into a gas pore. For a granular material, the pore size is of the order of the grain diameter, while the solid sound speed, $c_s \approx 3\,\mathrm{mm}/\mu\mathrm{s}$, provides a rough estimate of the transverse velocity. Thus, the time scale for pressure equilibrium could be as small as $\Delta t \sim 0.03\,\mu\mathrm{s}$. This is one reason why standard two-phase fluid models assume pressure equilibrium.

While weak compaction waves have smooth profiles and are fully dispersed, strong compaction waves contain shocks and are only partially dispersed. However, because of the narrow wave width, it is the state at the end of the pressure relaxation layer rather than that behind the shock discontinuity that is physically meaningful. This motivates us to develop a reduced model with a single pressure field, wherein the entire compaction wave will appear as a discontinuity.

3.3 Thermal-equilibration scales

If velocity and pressure equilibrium are accompanied by a state of thermal equilibrium as well, then the two-phase model collapses to the standard ZND model of an explosive in which a single-phase material has an extra degree of freedom corresponding to the mass fraction of the detonation products, $\lambda = \phi_g \rho_g / \rho$, and an equation of state based on pressure and temperature equilibrium [25]. However, as shown below, the thermal time scale is large and temperature equilibrium is not physically justified for the problems of interest.

The time scale for conductive transport is

$$\tau_t \sim \frac{\rho C_v}{\kappa} L^2 \ ,$$

where ρ is the density, C_v the specific heat, κ the coefficient of thermal conductivity, and L the characteristic length scale. From the energy equations, Eq. (14) or Eq. (15), the characteristic time for thermal transport is given by

$$\tau_t \sim \phi \rho C_v / \mathcal{H} \ .$$

Consequently, the coefficient for heat transfer is estimated to be

$$\mathcal{H} \sim \phi \kappa / L^2 \ .$$

This is similar to the form used by BN [1, Eq. (72)], when the Reynolds number based on the relative velocity is set to zero.

There are two limiting cases to consider: (i) the gas phase dominates the heat capacity, as occurs after sufficient combustion leads to a high gas temperature and at least a moderate gas mass fraction; and (ii) the solid phase dominates the heat capacity, as is the case near the initial state because the gas mass fraction is small. The parameters for HMX from [1] are $C_{vs} = 1.05 \times 10^7\,\mathrm{erg}/(\mathrm{g}\cdot\mathrm{K})$ and $\kappa_s = 4.0 \times 10^4\,\mathrm{erg}/(\mathrm{cm}\cdot\mathrm{s}\cdot\mathrm{K})$ for the solid phase, and $C_{vg} = 2.4 \times 10^7\,\mathrm{erg}/(\mathrm{g}\cdot\mathrm{K})$ and $\kappa_g = 7.0 \times 10^3\,\mathrm{erg}/(\mathrm{cm}\cdot\mathrm{s}\cdot\mathrm{K})$ for the gas phase.

In the first case, the gas pore acts as a heat reservoir for the solid grain. The natural length scale is half the grain size (0.1 mm) or $L_s \sim 5 \times 10^{-3}\,\mathrm{cm}$. With $\rho = 1.9\,\mathrm{g/cm^3}$, the thermal time scale of the solid is $\tau_{ts} \sim 18\,\mathrm{ms}$. This is long compared to the the time scale of a DDT experiment $\sim 100\,\mu\mathrm{s}$. Therefore, the solid is not expected to be in thermal equilibrium with high temperature burned gas.

For the second case, the solid acts as a heat reservoir for the gas. The length scale now depends on the porosity and an assumption on the shape of the gas pores

$$L_g \sim (\phi_g/\phi_s)^{\frac{1}{n}} L_s \ ,$$

where $n = 1, 2, 3$ corresponds to planar, cylindrical and spherical pores, respectively. It follows that the gas time constant is given by

$$\tau_{tg}/\tau_{ts} = [\lambda_g/(1-\lambda_g)] \cdot (C_{vg}/C_{vs}) \cdot (\kappa_s/\kappa_g) \cdot (\phi_g/\phi_s)^{\frac{2}{n}-1} \ .$$

where $\lambda_g = \phi_g\rho_g/\rho$ is the gas mass fraction. At an early stage in the DDT tube experiments, for $\lambda_g < 0.01$ and $\phi_s < 0.95$, the gas time constant is at least 1 ms.

These estimates indicate that thermal equilibrium between the bulk temperatures of the two phases occurs too slowly to be relevant on the time scales of interest. Heat conduction does affect the surface temperature of a grain and thus can be important when the burn rate is dominated by surface burning. However, to include effects of this nature requires, once again, a subscale model designed for the purpose; see Baer and Nunziato [15]. Key physical quantities likely to play a role here are the surface-to-volume ratio of the explosive grains and the flame stand-off distance relative to the pore size; see Son, Asay and Bdzil [26].

3.4 Relaxation effects

The above estimates of characteristic lengths and times demonstrate that the corresponding relaxation zones are very narrow, and as a result, the model is quite stiff. Typically, velocity and pressure disequilibrium occur immediately behind a shock front. This gives rise to a partly dispersed shock wave consisting of a discontinuous shock front followed by a thin relaxation zone in which equilibrium is re-established. An important consequence of relaxation, as we shall see, is the diminution of wave speed for a fixed pressure behind the wave, a necessary condition for stability. This is in accord with a general property of thermodynamic systems, *i.e.*, the equilibrium sound speed is less than the frozen sound speed. Disequilibrium also occurs in the profile of a weak, fully dispersed shock, in which dissipation from the relaxation process is sufficient to obtain a continuous wave profile. Fully dispersed shocks have a wave speed that lies between the equilibrium and frozen sound speeds.

From a practical point of view the detailed structure of a fully or partly dispersed wave is not important, but the state behind it and the wave speed are. Accurate calculation of these quantities, however, requires the fine relaxation structures to be accurately resolved as well, thereby adding needless expense to the computational process. It would be far more efficient to compute with reduced models for which velocity and pressure equilibrium are assumed to hold. Furthermore, in the limit that the relaxation zones shrink to zero, a fully or partly dispersed wave becomes a discontinuity or a shock wave in the reduced model. We now demonstrate how these reductions can be derived by means of an asymptotic analysis based on the formal sequential limits of infinite drag and zero compaction viscosity.

4 Velocity Equilibration: $\delta \to \infty$

For the purposes of this section, we take the 7-equation BN model to consist of the phase-specific mass and energy balance equations, Eqs. (1), (2), (5) and (6), the compaction law, Eq. (7), the mixture momentum equation, Eq. (26) and the velocity-difference equation, derived via simple algebraic manipulations from the phase-specific mass and momentum balance equations and given below:

$$\frac{\partial}{\partial t}\Big(u_s - u_g\Big) + \frac{\rho}{\phi_s\rho_s\phi_g\rho_g}\delta(u_s - u_g) = \frac{\partial}{\partial x}\left[\frac{\phi_s\rho_s - \phi_g\rho_g}{2\rho}(u_s - u_g)^2 - u(u_s - u_g)\right] + \frac{1}{\phi_s\rho_s\phi_g\rho_g}\left[\tfrac{1}{2}(\phi_s\rho_s - \phi_g\rho_g)(u_s - u_g)\mathcal{C} + \phi_s\rho_s\frac{\partial}{\partial x}(\phi_g P_g) - \phi_g\rho_g\frac{\partial}{\partial x}(\phi_s P_s) + \rho P_g\frac{\partial\phi_s}{\partial x}\right]. \quad (29)$$

This equation shows that velocity difference is promoted by gradients of pressure and porosity, but resisted by drag. At low gas densities burning acts in concert with drag (recall that $\mathcal{C} < 0$).

Strictly speaking, the large-drag reduction should begin with a dimensionless form of the governing equations, in which the drag parameter δ appears in a dimensionless group L_d^*/L^*, where L^* is an appropriate macroscopic length scale, and L_d^* the much smaller velocity-equilibration length

scale, given in terms of a reference density ρ_d^* and a reference velocity u_d^* by $L_d^* = \rho_d^* u_d^*/\delta$. The reduction is then obtained in the limit $L_d^*/L^* \to 0$. However, bowing to custom in the field, we retain the dimensional form of the equations and apply the limit $\delta \to \infty$ to achieve the same result. Each variable ψ is assumed to have the asymptotic expansion $\psi \sim \psi^{(0)} + \delta^{-1}\psi^{(1)} + \cdots$. The superscript (0) is omitted from the leading term to minimize clutter, so that henceforth, ψ will represent the leading term in its own asymptotic expansion unless specified otherwise.

As $\delta \to \infty$, in *outer* regions of the flow characterized by temporal and spatial gradients of order unity and the absence of very strong burning, the velocity-difference equation, Eq. (29), reduces at leading order to

$$u_s - u_g = 0,$$

i.e., the velocities of the two phases are the same at order unity. Accordingly, we set

$$u_s = u_g = u. \tag{30}$$

Moreover, velocity equilibrium is a stable flow configuration since the coefficient of $\delta(u_s - u_g)$ in Eq. (29) is positive. At the next order, Eq. (29) yields

$$u_s^{(1)} - u_g^{(1)} = \frac{1}{\rho}\left[\phi_s\rho_s\frac{\partial}{\partial x}(\phi_g P_g) - \phi_g\rho_g\frac{\partial}{\partial x}(\phi_s P_s)\right] + P_g\frac{\partial\phi_s}{\partial x}. \tag{31}$$

Note that the leading-order velocity difference is $O(\delta^{-1})$, and is related to, and indeed determined by, the $O(1)$ solution. Also, the product $\delta(u_s - u_g)$ makes an $O(1)$ contribution to the exchange terms and, thus, can not be taken as zero in smooth regions of the flow.

Our interest lies in developing a reduced model that holds at order unity. For the most part, this entails setting the velocity difference to zero in the remaining equations. The sole exception is the energy transfer term, Eq. (12), which to leading order assumes the reduced form

$$\tilde{\mathcal{E}} = \left(E_s + \beta_s V_s\right)\mathcal{C} + (u_g^{(1)} - u_s^{(1)})u + \left(T_g - T_s\right)\mathcal{H}\,, \tag{32}$$

in which the drag related term $u_g^{(1)} - u_s^{(1)}$ appears explicitly. Simply setting the drag term to zero is not consistent. It may, however, be eliminated in favor of order-unity terms by employing (31).

An alternative is to consider the phase-specific equations for internal energy alone, (14) and (15), in which the drag term, $\delta(u_s - u_g)^2$, is of higher order and thus negligible, thereby yielding a well-defined limit in which only $O(1)$ terms appear. In view of the arguments given above, the BN model reduces, in the limit of large drag, to the following set of six equations:

Mass balance

$$\frac{\partial}{\partial t}\Big(\phi_s\rho_s\Big) + \frac{\partial}{\partial x}\Big(\phi_s\rho_s u\Big) = \mathcal{C}, \tag{33}$$

$$\frac{\partial}{\partial t}\Big(\phi_g\rho_g\Big) + \frac{\partial}{\partial x}\Big(\phi_g\rho_g u\Big) = -\mathcal{C}; \tag{34}$$

Mixture momentum balance

$$\frac{\partial}{\partial t}\Big(\rho u\Big) + \frac{\partial}{\partial x}\Big(P + \rho u^2\Big) = 0, \tag{35}$$

Internal energy balance

$$\frac{\partial}{\partial t}\Big(\phi_s\rho_s e_{sp}\Big) + \frac{\partial}{\partial x}\Big(\phi_s\rho_s u e_{sp}\Big) + \phi_s P_s\frac{\partial u}{\partial x} = e_{sp}\,\mathcal{C} - (T_s - T_g)\mathcal{H} - (P_g + \beta_s)\mathcal{F}. \tag{36}$$

$$\frac{\partial}{\partial t}\Big(\phi_g\rho_g e_g\Big) + \frac{\partial}{\partial x}\Big(\phi_g\rho_g u e_g\Big) + \phi_g P_g\frac{\partial u}{\partial x} = -(e_{sp} + B + \beta_s V_s)\,\mathcal{C} + (T_s - T_g)\mathcal{H} + P_g\mathcal{F}\,. \tag{37}$$

Compaction dynamics

$$\frac{\partial}{\partial t}\rho_s + \frac{\partial}{\partial x}\left(\rho_s u\right) = -\frac{\rho_s}{\phi_s}\mathcal{F}\,. \tag{38}$$

An alternate form of the compaction equation, obtained by applying the reduction to Eq. (13), is

$$\frac{\partial \phi_s}{\partial t} + u\frac{\partial \phi_s}{\partial x} = \mathcal{F} + \frac{\mathcal{C}}{\rho_s}\,. \tag{39}$$

In lieu of Eqs. (36) and (37) above, balance of *total* energy for each phase would have led to the alternate pair:

Total energy balance

$$\frac{\partial}{\partial t}\Big[\phi_s\rho_s\big\{e_{sp} + B + \tfrac{1}{2}u^2\big\}\Big] + \frac{\partial}{\partial x}\Big[\phi_s u\Big(\rho_s\big\{e_{sp} + B + \tfrac{1}{2}u^2\big\} + P_s\Big)\Big] = -P_g\mathcal{F} + \tilde{\mathcal{E}}'\,, \tag{40}$$

$$\frac{\partial}{\partial t}\Big[\phi_g\rho_g\big\{e_g + \tfrac{1}{2}u^2\big\}\Big] + \frac{\partial}{\partial x}\Big[\phi_g u\Big(\rho_g\big\{e_g + \tfrac{1}{2}u^2\big\} + P_g\Big)\Big] = P_g\mathcal{F} - \tilde{\mathcal{E}}'\,, \tag{41}$$

with

$$\tilde{\mathcal{E}}' = \big(e_{sp} + B + \beta_s V_s + \tfrac{1}{2}u^2\big)\,\mathcal{C} + (T_g - T_s)\mathcal{H} - \frac{u}{\rho}\Big[\phi_s\rho_s\frac{\partial}{\partial x}(\phi_g P_g) - \phi_g\rho_g\frac{\partial}{\partial x}(\phi_s P_s)\Big]\,. \tag{42}$$

For either choice, it is noteworthy that the nozzling terms no longer play any role. Though the total energy, given by Eq. (27), is a conserved quantity, there are no physical conservation laws for the individual phase energies. Neither the internal nor the total energy balance equations for the individual phases can be put in conservation form.

An appropriate choice of state variables for the above form of the reduced model is the list $\mathcal{L}_1 : u, \phi_s, \rho_s, P_s, \rho_g, P_g$. One could also replace gas density and gas pressure by the corresponding mixture variables, leading to the alternate list $\mathcal{L}_2 : u, \phi_s, \rho_s, P_s, \rho, P$. For this choice, the gas mass balance law, Eq. (34), must be replaced by the mixture mass balance law, Eq. (25), and the gas energy balance, Eq. (37) or Eq. (41), must be replaced by the reduced form of the mixture energy balance equation,

$$\frac{\partial}{\partial t}\Big[\rho\Big(e + \tfrac{1}{2}u^2\Big)\Big] + \frac{\partial}{\partial x}\Big[\rho u\Big(e + \tfrac{1}{2}u^2\Big) + Pu\Big] = 0. \tag{43}$$

Some observations about the character of the reduced model are in order. First, we reiterate that the reduction is a limiting form of the BN-model, and as such, is valid only outside certain thin regions of large gradients. Second, while the solid entropy, Eq. (16), for the full model is devoid of any contribution from drag, this is true only at leading order for the gas entropy, Eq. (17). These equations reduce to

$$\phi_s\rho_s T_s\frac{d\eta_s}{dt} = \frac{\phi_s\phi_g}{\mu_c}(P_s - P_g - \beta_s)^2 - (T_s - T_g)\mathcal{H}\,, \tag{44}$$

$$\phi_g\rho_g T_g\frac{d\eta_g}{dt} = (T_s - T_g)\mathcal{H} - \big[H_s - H_g - (P_s - P_g - \beta_s)V_s\big]\mathcal{C}\,. \tag{45}$$

Thus the reduction confines all drag-related dissipation to the thin relaxation zones.

Third, it is shown in Appendix A that the reduced model is hyperbolic, with characteristic velocities u (4-fold) and $u \pm c$, c being an average sound speed of the mixture, defined in terms of the phase-specific frozen sound speeds c_s and c_g as

$$c^2 = (\phi_s\rho_s c_s^2 + \phi_g\rho_g c_g^2)/\rho. \tag{46}$$

Thus there exists a single pair of acoustic modes appropriate for the mixture, rather than a separate pair for each phase in the full model. Since c^2 is the mass-weighted average of c_s^2 and c_g^2, c has a value between c_s and c_g. Typically, the solid phase has a higher sound speed than the gas, so that

$$c_g < c < c_s \ .$$

This condition has been referred to as the subcharacteristic condition, and is a common property of stable relaxing systems [27, 12].

Fourth, although hyperbolic, only five of the six equations comprising the reduced model, those of mass, momentum and energy balance for the mixture, mass balance for the solid, and compaction, are in conservative form. It is possible to replace the solid energy equation with an equation in conservation form for the solid entropy,

$$\frac{\partial}{\partial t}\Big(\phi_s\rho_s\eta_s\Big) + \frac{\partial}{\partial x}\Big(\phi_s\rho_s u\eta_s\Big) = \eta_s\mathcal{C} + \frac{\phi_s\phi_g}{\mu_c T_s}(P_s - P_g - \beta_s)^2 - \frac{T_s - T_g}{T_s}\mathcal{H} \ .$$

The derived jump conditions would be compatible with thermodynamics, since across a shock the gas entropy and hence the total entropy would increase. Moreover, as shown in [13], [16] and reiterated below, for weak fully dispersed shocks the solid is indeed isentropic. However, as the shock strength increases the detailed analysis in [13] shows that a shock in the solid is required when the shock speed exceeds the solid sound speed. Therefore, expressing the reduced model completely in conservation form is untenable. We are forced to use the solid energy equation. Regardless of whether one chooses the internal-energy form, Eq. (36), or the total-energy form, Eq. (40), not all of the spatial derivatives therein can be expressed as gradients of fluxes. Across a discontinuity, therefore, the phase-specific energy equation does not reduce to an algebraic statement relating the states on the two sides of the discontinuity. Such a statement would require evaluation of such integrals as

$$\int \phi_s P_s \frac{\partial u}{\partial x}\, dx$$

or

$$\int \frac{u}{\rho}\left[\phi_s\rho_s\frac{\partial}{\partial x}(\phi_g P_g) - \phi_g\rho_g\frac{\partial}{\partial x}(\phi_s P_s)\right]\, dx$$

across the discontinuity, which can only be done by providing additional information about the structure of the discontinuity. If one were to employ a computational approach involving, say, artificial dissipation, then the end states would depend upon the nature of the dissipation introduced, and in particular on the manner in which dissipation were partitioned between the phases. Thus the reduced model is incomplete as it stands, and requires a *regularization* to select the admissible shock waves. Though the regularization is non-unique, physics dictates that across a shock the entropy jump in each phase must be non-decreasing, and for a strong shock the entropy of each phase should in fact increase. This constraint is analogous to the entropy inequality used in [7] to formulate the source terms for the full BN model. The non-uniqueness reflects the degree of freedom available to apportion shock energy between the phases.

We conclude this section with some remarks about higher-order terms in the asymptotic expansion of the solution in powers of δ^{-1}, even though we shall be content with just the leading term. One may envisage an iterative approach in which higher-order terms are computed from a recursive set of equations, of form

$$\mathbf{L}w_{n+1} = \mathbf{C}w_n \ ,$$

where $w_n = w^{(0)} + \sum_{i=1}^{n} \delta^{-i} w^{(i)}$ is the n^{th} partial sum of the asymptotic expansion of the solution vector w. As noted in [12], $\mathbf{L}$ is the operator associated with the reduced model while the correction $\mathbf{C}$,

depending only on lower-order terms, acts as a source. Correction signals from the higher-order terms flow along subcharacteristics and causality (domains of dependence and regions of influence) is maintained. There is a complication arising from the fact that signals from the correction sources propagate to the shock fronts. The shock velocity and hence the position of the corrected shock front will vary slightly; as a consequence, the source correction between the old and the new positions of the shock could be on the wrong side of the front. This involves only a small neighborhood and the error, based as it is on the integral of the sources, is bound to be small as well. However, its effect may accumulate and prevent error estimates from being uniform over long times.

Additionally, to obtain a complete asymptotic solution of the full model, the outer solution must be matched to thin inner layers characterized by gradients of order $O(\delta)$. The leading-order solution to the inner layer corresponds to steady wave profiles. At the next order the inner solution determines the quasisteady evolution of the wave, or the variation of the wave profile on a slow time scale compared to the rise time of the wave. The boundary condition for the inner solution must come from matching with the outer solution. Because the reduced model is hyperbolic, the flow of information dictates that boundary condition for the inner layer is determined by the incoming characteristic from the outer solution. In the limit $\delta \to 0$ the width of the inner zone shrinks to zero and corresponds to a shock wave of the reduced model. As a result, jump conditions provided by the leading order solution to the inner layer provide a regularization of the reduced model. Furthermore, this regularization reflects dissipation in the full model, which is thermodynamically consistent.

4.1 The inner layer

A different, inner approximation holds in narrow relaxation zones that are layers of width $O(1/\delta)$, and in which velocity differences can be of order unity. We now demonstrate how the leading-order solution of the inner layer determines the jump conditions for the outer layer.

On the scale of the outer spatial coordinate, suppose an inner layer appears at the location $x_w(t)$, with $\dot{x}_w = D(t)$. Here the "dot" denotes a time derivative. Within the layer the appropriate coordinates are t and the stretched variable $\xi = \delta(x - x_w)/m$, where the inclusion of m (the total mass flux through the zone, defined in Eq. (51) below) simply serves to make ξ dimensionless. We shall find it convenient to introduce velocities relative to a frame attached to the layer; thus, $\mathcal{U} = u - D$ with analogous definitions for $\mathcal{U}_s$ and $\mathcal{U}_g$. Then, in the new coordinates the compaction law, Eq. (7), transforms into

$$\frac{\partial}{\partial \xi}(\rho_s \mathcal{U}_s) = -\frac{m}{\delta}\left[\frac{\rho_s}{\phi_s}\mathcal{F} + \frac{\partial \rho_s}{\partial t} - \frac{\xi \dot{m}}{m}\frac{\partial \rho_s}{\partial \xi}\right].$$

We again seek asymptotic expansions in inverse powers of δ, with each variable representing the order-unity term in its own expansion as before. At leading order the above equation simply implies the constancy of $\rho_s \mathcal{U}_s$ in the inner layer. By an analogous argument, five of the seven governing equations, corresponding to mass conservation in each phase, momentum and energy conservation in the mixture, and as seen above, compaction, reduce at leading order to algebraic statements of conservation within the zone. These are

Mass conservation

$$\phi_s \rho_s \mathcal{U}_s = m_s, \quad \phi_g \rho_g \mathcal{U}_g = m_g, \tag{47}$$

Mixture momentum conservation

$$\phi_s P_s + \phi_g P_g + m_s \mathcal{U}_s + m_g \mathcal{U}_g = M, \tag{48}$$

Mixture energy conservation

$$m_s e_s + m_g e_g + \tfrac{1}{2} m_s \mathcal{U}_s^2 + \tfrac{1}{2} m_g \mathcal{U}_g^2 + \phi_s \mathcal{U}_s P_s + \phi_g \mathcal{U}_g P_g = E, \tag{49}$$

while the compaction condition $\rho_s \mathcal{U}_s =$ constant reduces, in view of Eq. (47) above, to simply

Compaction

$$\phi_s = \text{constant across the layer.} \tag{50}$$

The quantities m_s, m_g, M and E are, respectively, the conserved values of solid mass flux, gas mass flux, mixture momentum flux and mixture stagnation enthalpy flux across the zone. The phase-specific mass conservation equations, Eq. (47), imply mass conservation for the mixture, i.e.,

$$\rho \mathcal{U} = m_s + m_g \equiv m. \tag{51}$$

As the outer solution views the relaxation zone as a discontinuity, conservation of a quantity across the zone amounts to a zero jump in that quantity for the outer solution across the discontinuity. Recognizing that the inner solution must approach velocity equilibrium ($\mathcal{U}_s \to \mathcal{U}$, $\mathcal{U}_g \to \mathcal{U}$) as $\xi \to \pm\infty$, and following simple algebraic manipulations, the following jump conditions for the reduced model emerge upon matching at leading order across the zone:

$$\Big[\rho(u-D)\Big] = 0, \tag{52}$$

$$\Big[P + \rho u(u-D)\Big] = 0, \tag{53}$$

$$\Big[\rho(u-D)\left(e + \tfrac{1}{2}u^2\right) + Pu\Big] = 0, \tag{54}$$

$$\left[\frac{\rho_s}{\rho}\right] = 0, \tag{55}$$

$$\Big[\phi_s\Big] = 0. \tag{56}$$

These are precisely the five statements of conservation that are inherent in the reduced model and which we had referred to earlier. So far, the inner zone has not provided any additional information. For the one jump condition that still eludes us, we turn to the two equations in the inner zone that yet remain to be exploited. These correspond to energy and momentum balance for one of the phases, say the solid. Within the layer the solid momentum equation, Eq. (3), reduces to

$$\frac{\partial}{\partial \xi}[\phi_s P_s + m_s \mathcal{U}_s] = m(\mathcal{U}_g - \mathcal{U}_s). \tag{57}$$

Constancy of ϕ_s in the layer has eliminated the nozzling term while only the drag contribution from the momentum source $\tilde{\mathcal{M}}$ survives.

For the solid energy, we opt for the entropy form given by Eq. (16). For large δ the contributions from the source terms are negligible at leading order, yielding the simplified form

$$T_s \frac{d\eta_s}{d\xi} = 0,$$

implying that on the smooth portion of the relaxation-zone structure (*i.e.*, outside shocks), the solid isentrope

$$P_s = P_s(\rho_s, \eta_s) \tag{58}$$

applies. At a solid shock the appropriate entropy jump will need to be introduced.

The five conservation conditions, and the solid isentrope, leave only one variable yet to be determined in the layer via Eq. (57). We may take this variable to be the velocity difference $\mathcal{U}_s - \mathcal{U}_g$. A full solution of the structure equation, and the resulting jump conditions as a function of the speed D of the relaxation zone, were obtained in [13]. There it was shown that the minimum admissible

wave speed for the relaxation zone is c_0, the upstream value of the mixture sound speed. Further, the typical structure of the layer is monotonic, and involves hydrodynamic shocks in one or both phases. It is reminiscent of, but more complex than, what is seen in such simpler two-phase media as a dusty gas. For sufficiently weak waves, however, dissipation from drag is found to be sufficient for the wave profile to be continuous, *i.e.*, the shock is fully dispersed. In this special case, the solid entropy is constant across the layer and provides an additional algebraic condition that would enable the final state of the shock to be determined. But for stronger waves in which the wave profile has an embedded shock in the solid phase, an appropriate entropy jump across the shock has to be inserted.

While the BN regularization is satisfying from the viewpoint of its having supplied the requisite information, its numerical implementation is less than satisfactory if one wishes to employ a capturing rather than a tracking approach for the discontinuities. An alternate viewpoint would regard the equivelocity model not as a reduction, but in fact as a fundamental continuum description in its own right, one that lacks certain information about the manner in which energy dissipation is distributed between the phases on passage through the relaxation zone. One would then need to supply a subscale model with which to partition the shock mixture energy between the solid and gas internal energy for the reduced model. The BN model, through the structure of the relaxation zone, does provide such a closure. Another possibility would be to extract the desired information by averaging the results of a highly resolved microscale calculation that faithfully modeled the physics. This information could then be used to construct, for example, a viscous regularization, wherein appropriate artificial viscosities for each phase are introduced into the model, tailored so as to yield the jumps dictated by the microscale physics. Details of such a procedure, and supporting numerical computations, are slated to appear in our forthcoming paper [14].

5 Pressure Equilibration: $\mu_c \to 0$

Having derived what is effectively a one-velocity model, we now seek further reduction by turning to the second relaxation process for which the equilibration length scale has been estimated to be short, *i.e.*, compaction. The compaction law, Eq. (13), yields the estimate $L_c^* = \mu_c^* u_c^* / P_c^*$ for compaction length, where u_c^* and P_c^* are the characteristic scales for velocity and pressure in a compaction wave, respectively. The reduction corresponds to the limit $L_c^*/L^* \to 0$, where L^* is an appropriate macroscopic length scale. Equivalently, the reduction to a single pressure is appropriate when μ_c/P_c^* is small.

Just as had been done for velocity equilibration, it is instructive to develop an equation for the evolution of the pressure difference. To this end we take note of the thermodynamic relation

$$\Gamma de = (\gamma - \Gamma) P \, dV + V \, dP \ ,$$

where $\Gamma = V \partial P / \partial e \big|_V$ is the Grüneisen coefficient and $\gamma = \rho c^2 / P$ is the adiabatic exponent. Moreover, from Eq. (9) defining β_s and the solid mass balance, Eq. (33), we obtain

$$\frac{d\beta_s}{dt} = -\beta_s \frac{\partial u}{\partial x} + \frac{\beta_s}{\phi_s \rho_s} \mathcal{C} + \phi_s \rho_s \left(\frac{d^2 B}{d\phi_s^2} \right) \frac{d\phi_s}{dt} \ . \tag{59}$$

Simple algebraic manipulations on the phase-specific energy and mass equations, aided by the equation for compaction and thermodynamic relations, yield (alternatively, see Appendix A, Eqs. (112)

and (113))

$$\frac{d}{dt}\Big(P_s - P_g - \beta_s\Big) + \frac{\phi_s\phi_g}{\mu_c}\Big(P_s - P_g - \beta_s\Big)\left[\frac{\rho_s c_s^2}{\phi_s} + \frac{\rho_g c_g^2}{\phi_g} + \phi_s\rho_s\frac{d^2B}{d\phi_s^2} - \frac{\Gamma_s}{\phi_s}(P_s - P_g - \beta_s)\right]$$
$$= -\Big(\rho_s c_s^2 - \rho_g c_g^2 - \beta_s\Big)\frac{\partial u}{\partial x} - \left(\frac{\Gamma_s}{\phi_s} + \frac{\Gamma_g}{\phi_g}\right)(T_s - T_g)\mathcal{H}$$
$$+ \left[\frac{c_g^2}{\phi_g}\left(1 - \frac{\rho_g}{\rho_s}\right) + \frac{\Gamma_g}{\phi_g}\Big(H_s - H_g - (P_s - P_g - \beta_s)V_s\Big) - \frac{\beta_s}{\phi_s\rho_s} - \phi_s\frac{d^2B}{d\phi_s^2}\right]\mathcal{C}. \quad (60)$$

While the terms from heat transfer, burn and the acoustic-impedance differential between the phases can have either sign and therefore may or may not promote departure from equilibrium, we show that the compaction viscosity terms always serve to restore pressure equilibrium. The coefficient of the $(P_s - P_g - \beta_s)/\mu_c$ term can be expressed as

$$\big(\gamma_s - \Gamma_s\big)\frac{P_s}{\phi_s} + \frac{\rho_g c_g^2}{\phi_g} + \phi_s\rho_s\frac{d^2B}{d\phi_s^2} + \frac{\Gamma_s}{\phi_s}(P_g + \beta_s)\ . \quad (61)$$

Shock stability in multi-dimensions requires an equation of state to satisfy the condition $\gamma \geq \Gamma + 1$, see [28, §4.1] and references therein. Since compaction energy is a convex function, $d^2B/d\phi_s^2 \geq 0$. Consequently, every term in Eq. (61) is positive and the compaction viscosity term acts as a restoring force.

An asymptotic expansion of the equivelocity model, Eqs. (33)–(38), is now sought in the form $\psi \sim \psi^{(0)} + \mu_c\psi^{(1)} + \cdots$. For notational simplicity, the superscript (0) is omitted again from the $O(1)$ terms in the expansions. In outer regions of the flow, characterized by gradients that stay bounded in the limit $\mu_c \to 0$, the pressure-difference equation, Eq. (60), reduces to $P_s - P_g - \beta_s = 0$, allowing us to set

$$P_s = P + \phi_g\beta_s \qquad \text{and} \qquad P_g = P - \phi_s\beta_s\ , \quad (62)$$

where P is the mixture pressure, Eq. (22). Since compaction viscosity provides a restoring force, pressure equilibrium is a stable configuration.

At the next order nonequilibrium effects appear, producing an $O(\mu_c)$ imbalance given by

$$\phi_s\phi_g\Big(P_s^{(1)} - P_g^{(1)} - \beta_s^{(1)}\Big)\left[\frac{\rho_s c_s^2}{\phi_s} + \frac{\rho_g c_g^2}{\phi_g} + \phi_s\rho_s\frac{d^2B}{d\phi_s^2}\right] = -(\rho_s c_s^2 - \rho_g c_g^2 - \beta_s)\frac{\partial u}{\partial x}$$
$$+ \left[\frac{c_g^2}{\phi_g}\left(1 - \frac{\rho_g}{\rho_s}\right) + \frac{\Gamma_g}{\phi_g}\Big(H_s - H_g\Big) - \frac{\beta_s}{\phi_s\rho_s} - \phi_s\frac{d^2B}{d\phi_s^2}\right]\mathcal{C} - \left(\frac{\Gamma_s}{\phi_s} + \frac{\Gamma_g}{\phi_g}\right)(T_s - T_g)\mathcal{H} \quad (63)$$

The compaction equation, Eq. (39), now reduces to

$$\frac{d\phi_s}{dt} = \phi_s\phi_g\Big(P_s^{(1)} - P_g^{(1)} - \beta_s^{(1)}\Big) + \frac{\mathcal{C}}{\rho_s}. \quad (64)$$

Elimination of the pressure imbalance term between the last two equations leads to what essentially is a compaction-dynamics equation expressed entirely in terms of order unity quantities,

$$\frac{d\phi_s}{dt}\left[\frac{\rho_s c_s^2}{\phi_s} + \frac{\rho_g c_g^2}{\phi_g} + \phi_s\rho_s\frac{d^2B}{d\phi_s^2}\right] = -(\rho_s c_s^2 - \rho_g c_g^2 - \beta_s)\frac{\partial u}{\partial x} - \left(\frac{\Gamma_s}{\phi_s} + \frac{\Gamma_g}{\phi_g}\right)(T_s - T_g)\mathcal{H}$$
$$+ \left[\frac{c_s^2}{\phi_s} + \frac{c_g^2}{\phi_g} + \frac{\Gamma_g}{\phi_g}\Big(H_s - H_g\Big) - \frac{\beta_s}{\phi_s\rho_s}\right]\mathcal{C}\ . \quad (65)$$

The reduced model can now be taken to consist of the following five equations: the phase-specific mass balance equations, Eqs. (33) and (34), the mixture momentum equation, Eq. (35), the mixture energy equation, Eq. (43), and the compaction-dynamics equation, Eq. (65). In addition, the PDEs are to be supplemented with the algebraic pressure equilibrium condition, Eq. (62), and constitutive equations for the solid and gas phase. For convenience, the PDEs are gathered below.

Mass balance

$$\frac{\partial}{\partial t}\Big(\phi_s\rho_s\Big) + \frac{\partial}{\partial x}\Big(\phi_s\rho_s u\Big) = \mathcal{C}, \tag{66}$$

$$\frac{\partial}{\partial t}\Big(\phi_g\rho_g\Big) + \frac{\partial}{\partial x}\Big(\phi_g\rho_g u\Big) = -\mathcal{C}, \tag{67}$$

or alternatively

$$\frac{\partial \rho}{\partial t} + \frac{\partial(\rho u)}{\partial x} = 0, \tag{68}$$

$$\frac{\partial \lambda_s}{\partial t} + u\frac{\partial \lambda_s}{\partial x} = \frac{\mathcal{C}}{\rho}, \tag{69}$$

Mixture momentum balance

$$\frac{\partial}{\partial t}\Big(\rho u\Big) + \frac{\partial}{\partial x}\Big(P + \rho u^2\Big) = 0, \tag{70}$$

Mixture energy balance

$$\frac{\partial}{\partial t}\Big[\rho\left(e + \tfrac{1}{2}u^2\right)\Big] + \frac{\partial}{\partial x}\Big[\rho u\left(e + \tfrac{1}{2}u^2\right) + Pu\Big] = 0, \tag{71}$$

Compaction dynamics

$$\frac{d\phi_s}{dt}\left[\frac{\rho_s c_s^2}{\phi_s} + \frac{\rho_g c_g^2}{\phi_g} + \phi_s\rho_s\frac{d^2B}{d\phi_s^2}\right] = -(\rho_s c_s^2 - \rho_g c_g^2 - \beta_s)\frac{\partial u}{\partial x} - \left(\frac{\Gamma_s}{\phi_s} + \frac{\Gamma_g}{\phi_g}\right)(T_s - T_g)\mathcal{H} + \left[\frac{c_s^2}{\phi_s} + \frac{c_g^2}{\phi_g} + \frac{\Gamma_g}{\phi_g}\Big(H_s - H_g\Big) - \frac{\beta_s}{\phi_s\rho_s}\right]\mathcal{C}. \tag{72}$$

The five state variables appropriate for the reduction can be taken to be ρ_s, ρ_g, P, ϕ_s and u. The alternate form of the mass conservation equations, Eqs. (68) and (69), highlights the similarities of these reduced equations to the standard equations used when modeling shock-initiation of condensed phase explosives. Then the five state variables would be ρ, λ_s, P, ϕ_s and u. The variable ϕ_s, which doesn't appear in the standard set for modeling high explosives, is used in place of one of the individual energy equations. Importantly, these equations have inherited both mechanical (Galilean invariance) and thermodynamic consistency from the parent equations (the full BN model).

One could equally well replace P by the mixture internal energy e, in which case it is necessary to express P in terms of the state variables. This can be done analytically in the practically important case when a Mie-Grüneisen form of equation of state,

$$P_a(V_a, e'_a) = \mathcal{P}_a(V_a) + \frac{\Gamma_a}{V_a}e'_a \ ,$$

is used for both the solid and gas phase. In the above equation, $\mathcal{P}_a(V_a)$ describes the response of the material along a reference curve in the (P_a, V_a)–plane. Equation (23) for the mixture e and the pressure equilibrium condition give simultaneous equations for e_{sp} and e_g

$$\lambda_s e_{sp} + \lambda_g e_g = e - \lambda_s B \ , \tag{73}$$

$$\Gamma_s\rho_s e_{sp} - \Gamma_g\rho_g e_g = -\big[\mathcal{P}_s(V_s) - \mathcal{P}_g(V_g) - \beta_s\big] \ . \tag{74}$$

The solution is

$$e_{sp} = \frac{\Gamma_g\rho_g(e-\lambda_s) - \lambda_g\big[\mathcal{P}_s(V_s) - \mathcal{P}_g(V_g) - \beta_s\big]}{\Gamma_g\rho_g\lambda_s + \Gamma_s\rho_s\lambda_g} \ , \tag{75}$$

$$e_g = \frac{\Gamma_s\rho_s(e-\lambda_s) + \lambda_s\big[\mathcal{P}_s(V_s) - \mathcal{P}_g(V_g) - \beta_s\big]}{\Gamma_g\rho_g\lambda_s + \Gamma_s\rho_s\lambda_g} \ . \tag{76}$$

Substituting the phase energies into the equation of state gives the phase pressures

$$P_s = \frac{\Gamma_g\rho_g\lambda_s\mathcal{P}_s(V_s) + \Gamma_s\rho_s\Big(\Gamma_g\rho_g(e-\lambda_s B) + \lambda_g\big[\mathcal{P}_g(V_g) + \beta_s\big]\Big)}{\Gamma_g\rho_g\lambda_s + \Gamma_s\rho_s\lambda_g} \ , \tag{77}$$

$$P_g = \frac{\Gamma_s\rho_s\lambda_g\mathcal{P}_g(V_g) + \Gamma_g\rho_g\Big(\Gamma_s\rho_s(e-\lambda_s B) + \lambda_s\big[\mathcal{P}_s(V_s) - \beta_s\big]\Big)}{\Gamma_g\rho_g\lambda_s + \Gamma_s\rho_s\lambda_g} \ . \tag{78}$$

This leads to the desired expression for the mixture pressure in terms of the state variables,

$$P = \frac{\Gamma_g\rho_g\lambda_s[\mathcal{P}_s(V_s) - \phi_g\beta_s] + \Gamma_s\rho_s\lambda_g[\mathcal{P}_g(V_g) + \phi_s\beta_s] + \Gamma_g\rho_g\Gamma_s\rho_s(e-\lambda_s B)}{\Gamma_g\rho_g\lambda_s + \Gamma_s\rho_s\lambda_g} \ . \tag{79}$$

We now summarize the properties of this reduction. First, as shown in Appendix B, the reduction is hyperbolic. The characteristic velocities are u (3-fold) and $u \pm c_{\rm eq}$, where $c_{\rm eq}$ is the equilibrium sound speed, given by

$$\rho c_{\rm eq}^2 = \rho c^2 - \frac{\big(\rho_s c_s^2 - \rho_g c_g^2 - \beta_s\big)^2}{\frac{\rho_s c_s^2}{\phi_s} + \frac{\rho_g c_g^2}{\phi_g} + \phi_s\rho_s\frac{d^2B}{d\phi_s^2}} \ , \tag{80}$$

where c, defined in Eq. (46), is the mixture sound speed that emerged as a subcharacteristic of the velocity reduction alone. We require B to be convex and $\gamma_s > \gamma_g$. Then, as is typical for an equilibrium model, the equilibrium sound speed is reduced, *i.e.*, $c_{\rm eq} < c$. Since $u < u + c_{\rm eq} < u + c$, the subcharacteristic condition is satisfied.

It is interesting to note that $c_{\rm eq}$ takes its minimum value when the compaction potential B and configuration pressure β_s can be neglected; this minimum is given by

$$\frac{1}{\rho\,\tilde{c}_{\rm eq}^2} = \frac{\phi_s}{\rho_s c_s^2} + \frac{\phi_g}{\rho_g c_g^2} \ . \tag{81}$$

It can be shown that $\tilde{c}_{\rm eq} < c_g < c_s$ when $c_g < c_s$ and $\rho_g/\rho_s < \phi_g\phi_s$. Figure 1 shows an example in which the $c_{\rm eq}$ is less than the sound speed of either phase. This fact has been noted before, see, for example, [10, p. 381]. Incidentally, the single-phase limit of this model, corresponding to an absence of gas, describes the porous solid alone, for which the sound speed is given by Eq. (80) with $\rho_g = 0$ [29]. This limit is a variant of the well-known Herrmann-Carrol-Holt P–α model [30, 31].

Second, the entropy equations, Eqs. (44) and (45), reveal that in the broad regions of moderate gradients being considered here, the reduced model has no dissipation from compaction at leading order. Thus, the non-equilibrium degree of freedom associated with separate phase pressures has been eliminated. Compaction dissipation may only occur in narrow inner layers where gradients of ϕ_s are large. Even there, Eq. (45) shows that the gas remains isentropic, except in shocks or in thin zones of velocity disequilibrium that may form a part of the compaction wave.

Third, while the first four equations comprising the reduction, Eqs. (66) – (71), are in conservative form, the last, the compaction dynamics, given by Eq. (72), is not. As a result, there is only a partial

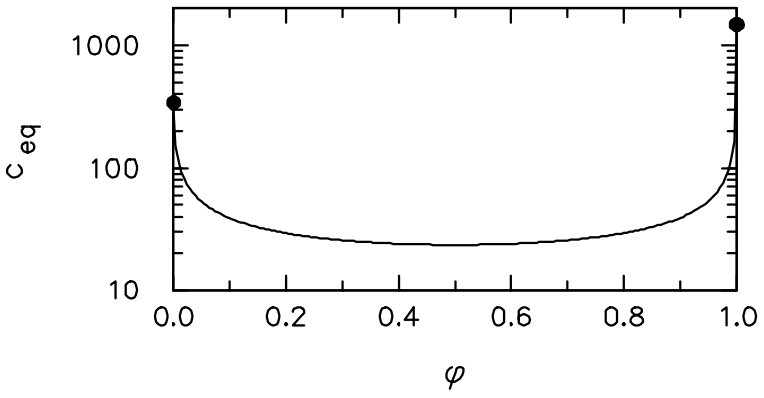

Figure 1: Equilibrium sound speed for air-water mixture as function of the volume fraction of water. Densities and sound speeds of each material are: $\rho_{\rm air} = 1.2\,{\rm kg/m^3}$, $c_{\rm air} = 340\,{\rm m/s}$; $\rho_{\rm water} = 1000\,{\rm kg/m^3}$, $c_{\rm water} = 1480\,{\rm m/s}$.

set of four jump conditions across a compaction discontinuity traveling at speed D :

$$\Big[\phi_s\rho_s(u-D)\Big] = 0, \tag{82}$$

$$\Big[\phi_g\rho_g(u-D)\Big] = 0, \tag{83}$$

$$\Big[P+\rho u(u-D)\Big] = 0, \tag{84}$$

$$\Big[\rho(u-D)\left(e+\tfrac{1}{2}u^2\right)+Pu\Big] = 0. \tag{85}$$

To close the system one needs additional information, and that requires a regularization to specify the admissible shock waves. A match with the solution in the thin compaction layer, provides a thermodynamically consistent regularization. An analysis of the inner layer is presented in the next subsection.

Weak compaction waves, with a wave speed in the range $c_{\rm eq} < D < c$, are fully dispersed, and may be too wide for the thin layer assumption used to derive an inner solution for a shock profile. The small amount of dissipation needed to obtain a fully dispersed wave results from the $\frac{\phi_s\phi_g}{\mu_c}(P_s - P_g - \beta_s)^2$ term in the solid entropy equation (44). This dissipative term vanishes in the reduced model. However, the compaction dissipation that enters in the next order of the asymptotic expansion can be incorporated into the reduced model in the simple manner employed by Chen, Levermore and Liu [12] in their analysis of hyperbolic PDEs with relaxation. Tracking a pressure imbalance from equation (74) to equation (79) would add a correction Q to the mixture pressure,

$$Q = \frac{\lambda_g\Gamma_s\rho_s\phi_s - \lambda_s\Gamma_g\rho_g\phi_g}{\Gamma_g\rho_g\lambda_s + \Gamma_s\rho_s\lambda_g}\Big(P_s^{(1)} - P_g^{(1)} - \beta^{(1)}\Big)\mu_c\,. \tag{86}$$

From (63) neglecting burning ($\mathcal{C} = 0$) and heat conduction ($\mathcal{H} = 0$), Q has the form of a viscous pressure

$$Q = -\mu_c\frac{\lambda_g\lambda_s(\Gamma_s - \Gamma_g)\rho}{\Gamma_g\rho_g\lambda_s + \Gamma_s\rho_s\lambda_g}\left(\frac{\rho_s c_s^2 - \rho_g c_g^2 - \beta}{\phi_g\rho_s c_s^2 + \phi_s\rho_g c_g^2 + \phi_g\phi_s^2\rho_s\frac{d^2}{d\phi^2}B}\right)\frac{\partial u}{\partial x}\,. \tag{87}$$

This viscous pressure provides the necessary dissipation to capture a weak fully dispersed compaction wave. Unlike artificial viscosity the viscous pressure from the leading order pressure imbalance

does not scale with the cell size. Sufficient resolution would be needed to resolve the wave width numerically. A regularization of the reduced model is still be needed to capture stronger shock waves which require more dissipation than compaction alone can provide.

5.1 The compaction layer

For algebraic convenience we opt to examine the inner layer when the compaction potential B and the configuration stress β_s are ignored. This approximation will, of course, become increasingly accurate at higher pressures when the strength of the grains is negligible. In order to determine the structure of the compaction layer (and more importantly, the pressure jump across it), one takes a step back and returns to the reduced model based on just the large-drag limit. The six independent equations comprising this model can be taken to be the two mass balances, the mixture momentum balance, the mixture energy balance, the gas internal energy balance and the compaction equation. The analysis is similar in spirit to that for the velocity-relaxation layer, summarized in section 4.1 above and performed in detail in [13]. Therefore, we present only the highlights here, relegating the algebraic details to Appendix C.

On the scale of the outer coordinate, consider a steady (left facing) compaction wave located at $x_c(t) = -Dt,\ D > 0$. Within the layer the stretched variable $\zeta = (x - x_c)m/\mu_c$ is appropriate, where the inclusion of the total mass flux m through the layer serves to make ζ dimensionless. Again we denote by $\mathcal{U}$ the particle velocity relative to the wave, *i.e.*, $\mathcal{U} = u + D$, and hence, $d/dt = \mathcal{U}d/d\zeta$.

The balance equations for mass, mixture momentum and mixture energy yield the algebraic conservation conditions,

$$\phi_s \rho_s \mathcal{U} = m_s \equiv \phi_{s0}\rho_{s0} D, \tag{88}$$

$$\phi_g \rho_g \mathcal{U} = m_g \equiv \phi_{g0}\rho_{g0} D, \tag{89}$$

$$\phi_s P_s + \phi_g P_g + m\mathcal{U} = P_0 + mD, \tag{90}$$

$$m\left(e + \tfrac{1}{2}\mathcal{U}^2\right) + P\mathcal{U} = E \equiv m\left(e_0 + \tfrac{1}{2}D^2\right) + P_0 D, \tag{91}$$

where

$$m \equiv \rho\mathcal{U} = \rho_0 D = m_s + m_g. \tag{92}$$

We have assumed that the compaction wave travels into a medium that is at rest (with respect to a laboratory frame), and that the upstream state is prescribed by $P_{s0},\ P_{g0},\ \rho_{s0},\ \rho_{g0},\ \phi_{s0}$ and ϕ_{g0}. Observe that

$$P_{s0} = P_{g0} = P_0. \tag{93}$$

since the state ahead of the wave is in pressure equilibrium and β_s has been ignored. Likewise, the neglect of B leads to the simpler form for the mixture internal energy,

$$e = \phi_s \rho_s e_{sp} + \phi_g \rho_g e_g.$$

Within the layer the compaction law, Eq. (39), reduces to

$$\mathcal{U}\frac{\partial \phi_s}{\partial \zeta} = \frac{\phi_s \phi_g (P_s - P_g)}{m}. \tag{94}$$

It remains to examine the gas-phase energy equation, Eq. (37), or equivalently, the gas-phase entropy equation, Eq. (45), which reduces, within the layer and at leading order, to

$$T_g \frac{\partial \eta_g}{\partial \zeta} = 0,$$

confirming that the gas compacts isentropically outside a shock. (It is a simple matter to see that the solid will behave differently.) Thus, on the smooth portion of the compaction-wave trajectory,

$$P_g = P_g(\rho_g, \eta_g), \tag{95}$$

where the precise form of the isentrope depends upon the gas EOS. The upshot is that the compaction wave is now governed by the four conservation statements, Eqs. (88 - 91), the gas isentrope, Eq. (95), and the compaction equation, Eq. (94). Only the last of these is a differential equation, so that one is only dealing with a first-order structure problem. We can use the four conservation statements to express ρ_s, ρ_g, P_s and P_g in terms of $\mathcal{U}$ and ϕ_s. The gas isentrope allows $\mathcal{U}$ to be eliminated, in principle, and then, the compaction equation, Eq. (94), yields the profile of ϕ_s across the compaction wave. If one is only interested in the jump conditions, one may replace the compaction equation by the pressure-equilibrium condition $P_s - P_g = 0$.

It is useful to render the problem dimensionless. We choose D to be the scale for velocity, ρ_0 for density, $\rho_0 D^2$ for pressure, and D^2 for energy. Scaled quantities will be denoted by an overbar. The conservation conditions then become

$$\phi_s \bar{\rho}_s \bar{\mathcal{U}} = \phi_{s0} \bar{\rho}_{s0}, \tag{96}$$

$$\phi_g \bar{\rho}_g \bar{\mathcal{U}} = \phi_{g0} \bar{\rho}_{g0}, \tag{97}$$

$$\phi_s \bar{P}_s + \phi_g \bar{P}_g + \bar{\mathcal{U}} = \bar{P}_0 + 1, \tag{98}$$

$$\bar{e} + \tfrac{1}{2}\bar{\mathcal{U}}^2 + \bar{P}\bar{\mathcal{U}} = \bar{e}_0 + \tfrac{1}{2} + \bar{P}_0, \tag{99}$$

while the compaction equation becomes

$$\bar{\mathcal{U}} \frac{\partial \phi_s}{\partial \zeta} = \phi_s \phi_g (\bar{P}_s - \bar{P}_g). \tag{100}$$

To make further progress we need to specify the equations of state. We take the gas to be polytropic and the solid to be a Tait material; these are both special cases of the Mie-Grüneisen form introduced earlier. Then the equations of state, and the corresponding sound speeds, in scaled forms, are

$$\bar{e}_g = \frac{\bar{P}_g}{(\gamma_g - 1)\bar{\rho}_g}, \quad \bar{c}_g^2 = \frac{\gamma_g \bar{P}_g}{\bar{\rho}_g}, \tag{101}$$

$$\bar{e}_s = \frac{\bar{P}_s + \gamma_s \bar{P}^*_{s0}}{(\gamma_s - 1)\bar{\rho}_s} - \frac{\gamma_s \bar{P}^*_{s0} + \bar{P}_{s0}}{(\gamma_s - 1)\bar{\rho}_{s0}}, \quad \bar{c}_s^2 = \frac{\gamma_s (\bar{P}_s + \bar{P}^*_{s0})}{\bar{\rho}_s}, \tag{102}$$

while the gas isentrope through the initial state is given by

$$\frac{\bar{P}_g}{\bar{P}_{g0}} = \left(\frac{\bar{\rho}_g}{\bar{\rho}_{g0}} \right)^{\gamma_g}. \tag{103}$$

The procedure for computing the end state behind the compaction zone is now straightforward, and we describe it very briefly. One begins by solving Eqs. (96) and (97) for the densities $\bar{\rho}_s$, $\bar{\rho}_g$, which, when substituted into Eqs. (98) and (99), yielding expressions for the pressures $\bar{P}_s$, $\bar{P}_g$ in terms of ϕ_s and $\mathcal{U}$. On equating the two pressures, one obtains the pressure-equilibrium locus $\mathcal{L}_E$ in the ϕ_s,$\mathcal{U}$-plane (Eq. (144) in Appendix C). Likewise, the gas isentrope, Eq. (103), is also expressed as a locus $\mathcal{L}_I$ in the ϕ_s,$\mathcal{U}$-plane (Eq. (147) in Appendix C). Both the loci originate at the point $\phi_s = \phi_{s0}$, $\mathcal{U} = 1$, corresponding to the state upstream. The locus $\mathcal{L}_I$ is, in fact, the trajectory of the compaction wave, and its (second) intersection with the equilibrium locus yields the end state.

The minimum wave speed for which the two loci have a second intersection is found to be

$$D_{\min} = c_{\mathrm{eq}0}, \tag{104}$$

quantity	value	
ϕ_{s0}	0.75	
γ_s	3	
γ_g	1.25	
c_{s0}	1088	m/s
c_{g0}	422	m/s
ρ_{s0}	1900	kg/m^3
ρ_{g0}	0.7	kg/m^3
P_{s0}	10^5	Pa
P_{g0}	10^5	Pa
c_0	1088	m/s
c_{eq_0}	18.7	m/s

Table 1: Upstream state for end state calculation.

which corresponds to the equilibrium sound speed of the mixture at the state upstream. As D is increased above the minimum, the strength of the wave, as measured by, say, the jump in the solid volume fraction $\phi_s - \phi_{s_0}$, also increases from zero. The wave has a dispersed, smooth profile, until the wave speed reaches the critical value

$$D_{\mathrm{crit}} = c_0, \tag{105}$$

where c_0 is the mixture sound speed appropriate for velocity equilibrium, again evaluated at the state upstream.

We recall that c_0 is also the *minimum* wave speed at which a velocity discontinuity will travel in the equivelocity reduced model. At speeds $D > c_0$, therefore, the compaction layer must be preceded by a velocity-discontinuity at its head, across which velocity, pressure and gas entropy will jump, while the volume fraction stays fixed at the upstream value ϕ_{s_0}. The state immediately behind such a discontinuity will be one of equal velocities but unequal pressures, and is given by the analysis in [13]. Denote it by, say, the point $(\bar{\mathcal{U}}_*, 0)$ in the $\bar{\mathcal{U}}, \phi$-plane, where $\bar{\mathcal{U}}_*$ is a function of the wave speed D. The compaction wave, immediately following the velocity discontinuity, will have its trajectory along a new gas isentrope emerging from the point $(\bar{\mathcal{U}}_*, 0)$, terminating as before at the equilibrium locus. Thus, compaction dissipation suffices to render structures of compaction waves traveling below D_{crit} as continuous, while those traveling above D_{crit} involve velocity shocks.

For illustrative purposes, we now present an end state calculation for a representative compaction wave that travels into a granular mixture at equilibrium under atmospheric conditions. The state of each phase upstream of the wave, including the relevant sound speeds for the mixture, are listed in table 1. The configuration stress β_s is ignored, in line with the discussion above. Figure 2 illustrates the (dimensional) velocity $\mathcal{U}$, pressure P and the degree of compaction $\phi \equiv (\phi_s - \phi_{s_0})/(1 - \phi_{s_0})$ behind the wave. We note that as the wave speed D is increased from the minimum admissible value of 18.7 m/s to 400 m/s, the compaction rises nearly to unity, long before the upper limit of 1088 m/s for a smooth compaction profile is reached. This is a consequence of neglecting the configuration stress.

6 Final Remarks

Starting with the two-phase Baer-Nunziato model, in which distinct velocities and pressures are associated with each phase, we derive two reductions: one with a single velocity and the other with a single velocity and a single pressure. The reductions are based upon careful estimation of the

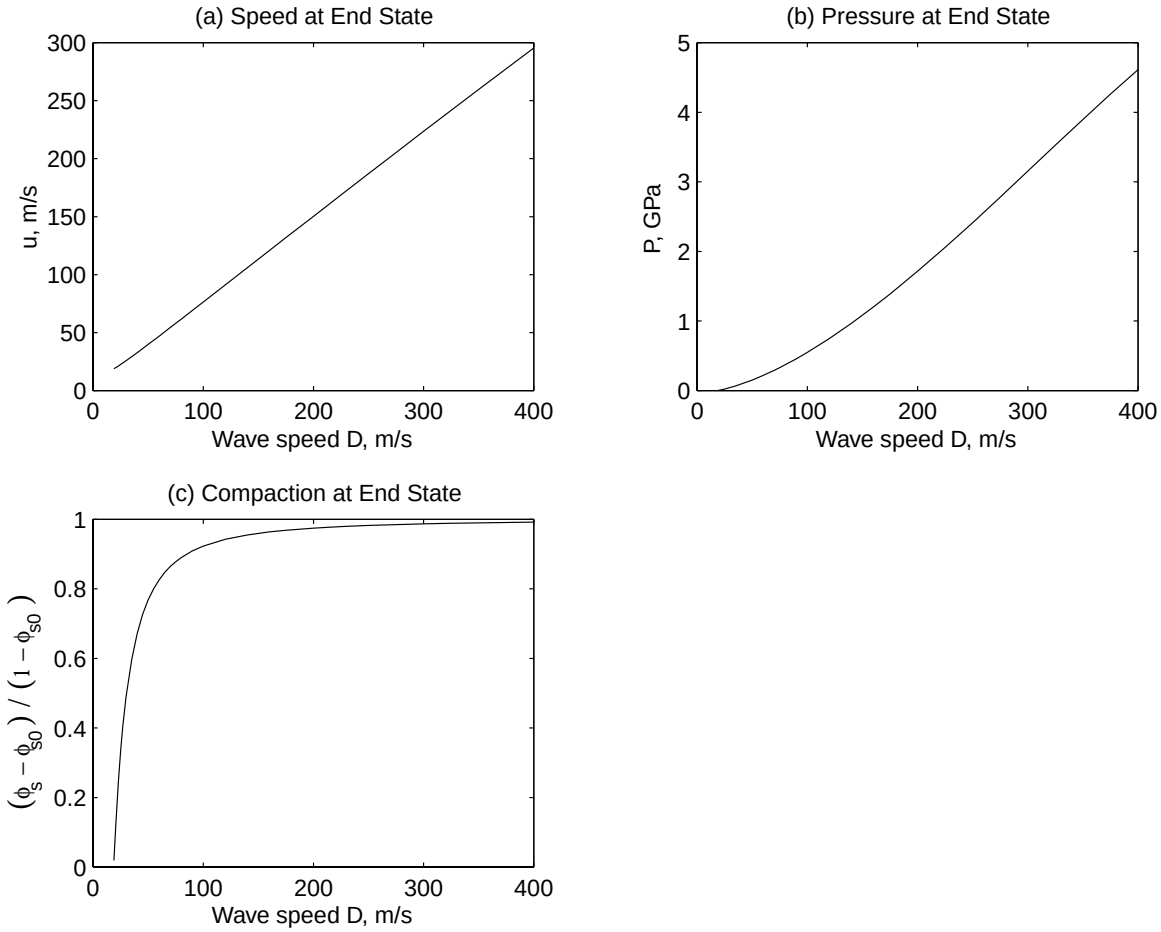

Figure 2: State behind compaction wave: a) dimensional velocity, b) pressure, and c) degree of compaction.

underlying rate processes of drag and compaction, which are found to be stiff. Each reduction is associated with a relaxation process, and eliminates a non-equilibrium degree of freedom. The reduced equations constitute leading-order outer expansions of the full model, valid in broad regions where gradients are $O(1)$. Supplementary inner expansions describe narrow regions with large gradients, where nonequilibrium prevails and to which all the dissipation associated with the relaxation processes is confined, at leading order. In the limits of large drag, $\delta \to \infty$, and small compaction viscosity, $\mu_c \to 0$, the inner layers shrink to zero width and correspond to shock waves in the reduced models.

The reduced models are hyperbolic but cannot be cast completely in conservation form. This has important implications, not the least for numerical simulations. First, in any computation with the full model, accurate jump conditions across a relaxation layer require that the layer be resolved (both temporally and spatially) with sufficient fidelity. Stiffness of the relaxation source terms make this an expensive undertaking, leading to incorrect solutions when the equilibration layers are not adequately resolved. Typically, such layers follow a shock wave, leading to what amounts to a partly dispersed shock wave. Thus, in contrast with standard shock capturing, where the end state of the shock is independent of the wave profile, numerical errors associated with a partly dispersed wave profile can affect the end state of the shock. Second, the reduced models are incomplete. A

regularization is needed to fully specify the jumps across a shock wave.

Regularization may be viewed, and implemented, in a number of ways. The full model itself provides one path to regularization. Asymptotic analyses of the structure equations for the inner layers, carried out here and in [13], yield the necessary jumps, which may then be used in conjunction with a front-tracking algorithm when computing with the reduced models.

An alternative is to treat the reduced models themselves as fundamental. Then, the full model plays the role of an enlarged equation set, one in which relaxation source terms have been inserted to provide the dissipation needed to generate a numerically stable shock wave. This is the basis of the shock capturing scheme of Jin and Xin [32]. However, as already mentioned above, lack of a conservative form for the equation set makes the capturing approach for the full model impractical.

A preferred method of regularizing the reduced systems, in our view, is to employ a subscale model for dissipation due to the relaxation processes. Such a model can be based on an empirical fit to experimental data or to numerical data generated from simulations of the underlying material micro-structure, see for example [33]. The preference for a subgrid model stems from the fact that the width of a strong wave is comparable to the heterogeneous length scale. A two-phase model represents a homogenization and without a subscale model would not describe the transient physics that occur in a shock profile. We also note that for a strong shock in a granular bed, both velocity and pressure equilibration take place on the scale of a few grains. In this case, the sequential limits of velocity equilibration followed by pressure equilibration is not appropriate.

It may also be possible to use artificial viscosities judiciously chosen so as to mimic the consequences of the microscale physics within the relaxation zones. In this connection, it is in order to mention the work of Sainsaulieu [34], who computes analytically the first terms of an asymptotic expansion for the jump conditions in the limit of vanishing viscosity. In a forthcoming paper [14] we perform an extensive series of numerical computations on the full BN model, and on regularized reduced models, to explore the feasibility and success of such regularization procedures.

It is interesting to note that the reduced model with a single velocity and a single pressure can be used to understand some of the difficulties that arise in an Eulerian algorithm for the Euler equations in a multi-component medium. The motion of interfaces between different materials leads to "mixed cells" or cells containing more than one material. Eulerian algorithms track the mass fraction of each component within a mixed cell. (Mass fraction is directly related to the volume fraction variable used in two-phase mixture theories.) These algorithms do not, however, track material interfaces within a cell. For the advection phase the interfaces are reconstructed, approximately, based on the volume of a component in a cell and in neighboring cells. But the interfaces are not used for the 'Lagrangian' time integration step. This step assumes that each cell has a single velocity and a single pressure. Some algorithms employ a mixed cell equation of state for the effective cell pressure, while others allow the components to have distinct pressures and use an average over the components for the cell pressure.

The mixed-cell equation of state is non-unique because of the degree of freedom associated with apportioning the cell energy between the components. (Recall that the time scale for temperature equilibration is much longer than that for pressure equilibration, and temperature equilibrium within a mixed cell is not justified.) When different pressures are allowed within a cell, a numerical relaxation is applied to equalize the component pressures, see [35] and [36]. The pressure relaxation amounts to adjusting the volume fraction and thus is analogous to the compaction law used in the BN model but with zero configuration pressure $\beta_s = 0$ and zero compaction energy $B = 0$. These schemes also attempt, at each time step, to distribute the PdV work done on each component within a mixed cell. Though this works well for isentropic flow and is reasonable for flows with weak shocks, these methods have difficulties with strong shocks. The difficulty with strong shocks is analogous to the regularization issue of the reduced model resulting from the non-conservative form of the equations. Physically, the regularization amounts to specifying how the shock energy is partitioned between the components.

Recently, Saurel & Abgrall [9] have developed a multi-component fluid algorithm based on a

system of PDEs for two-phase flow. Their equation set [9, Eq. (14)] is a slight variation of the two-phase BN model: (i) In the compaction equation (13), u_s is replace with the mixture velocity u. A similar substitution is made for the velocity that enters the drag source term and the nozzling term in the energy equations (5) and (6). (ii) For the compaction source term in the energy equation, P_g is replaced with the mixture pressure P. A similar substitution is made for pressure that enters the nozzling term in the momentum equations (3) and (4), and the energy equations (5) and (6). Saurel & Abgrall then use a small compaction viscosity and a large drag coefficient to establish pressure and velocity equilibrium between the components. The stiff relaxation source terms, in effect, leads to the reduced model that we have analyzed. Since the thin relaxation layers are captured and not resolved, the algorithm Saurel & Abgrall use relies on numerical dissipation to regularize the reduced model and select the shock waves. This may work for many applications, but as a matter of principle, the regularization should be part of the specification of the model and not arbitrarily selected by the algorithm used to implement the model.

Finally, we note that the lack of conservation form for the reduced model causes the BN model to lie outside the general theory of relaxation for hyperbolic conservation laws [12]. Nevertheless, the key properties of the general theory still hold; namely, the connection between the stability of the reduced model, the property that the subcharacteristic speeds interlace the characteristic speeds of the full model [27], and an entropy condition. This suggest that the relaxation theory of hyperbolic equations can be extended to cover a wider range of cases.

A Characteristics for Velocity Reduction

The velocity reduced model consists of the Eqs. (33)–(38). Here we express the reduced model in characteristic form. First we derive the four linear degenerate modes associated with the particle trajectory. For convenience we introduce the convective derivative $\frac{d}{dt} = \frac{\partial}{\partial t} + u\frac{\partial}{\partial x}$. The compaction equation, Eq. (39), is already in characteristic form.

$$\frac{d\phi_s}{dt} = \mathcal{F} + \frac{\mathcal{C}}{\rho_s}. \tag{106}$$

The phase energy equations can be replaced by those for entropy. From Eqs. (16) and (17), the entropy equations in the reduced model are

$$\phi_s\rho_s T_s\frac{d\eta_s}{dt} = (P_s - P_g - \beta_s)\mathcal{F} - (T_s - T_g)\mathcal{H}\,, \tag{107}$$

$$\phi_g\rho_g T_g\frac{d\eta_g}{dt} = (T_s - T_g)\mathcal{H} - \big[H_s - H_g - (P_s - P_g - \beta_s)V_s\big]\mathcal{C}\,. \tag{108}$$

The mass balance equations can be combined to yield

$$\frac{d}{dt}\Big(\frac{\phi_s\rho_s}{\phi_g\rho_g}\Big) = \frac{\rho\,\mathcal{C}}{(\phi_g\rho_g)^2}\ . \tag{109}$$

This can be expressed in terms of the solid mass fraction as

$$\frac{d}{dt}\Big(\frac{\phi_s\rho_s}{\rho}\Big) = \frac{\mathcal{C}}{\rho}\ . \tag{110}$$

To derive the acoustic mode we rewrite the mixture momentum balance as

$$\rho\frac{du}{dt} + \frac{\partial P}{\partial x} = 0. \tag{111}$$

Next we derive an equation for the pressure. Using the thermodynamic relation,

$$c^2 d\rho = dP - \Gamma\rho T d\eta\ ,$$

we can rewrite the mass balance equations as

$$\phi_s \frac{dP_s}{dt} + \phi_s \rho_s c_s^2 \frac{\partial u}{\partial x} = -\rho_s c_s^2 \frac{d\phi_s}{dt} + \Gamma_s \phi_s \rho_s T_s \frac{d\eta_s}{dt} + c_s^2 \mathcal{C}, \tag{112}$$

$$\phi_g \frac{dP_g}{dt} + \phi_g \rho_g c_g^2 \frac{\partial u}{\partial x} = \rho_g c_g^2 \frac{d\phi_s}{dt} + \Gamma_g \phi_g \rho_g T_g \frac{d\eta_g}{dt} - c_g^2 \mathcal{C} \, . \tag{113}$$

These can be combined to yield

$$\frac{dP}{dt} + \Big(\phi_s \rho_s c_s^2 + \phi_g \rho_g c_g^2\Big) \frac{\partial u}{\partial x} = \mathcal{S} \, . \tag{114}$$

where

$$\mathcal{S} = \Big[\big(P_s - \rho_s c_s^2\big) - \big(P_g - \rho_g c_g^2\big)\Big] \frac{d\phi_s}{dt} + \Gamma_s \phi_s \rho_s T_s \frac{d\eta_s}{dt} + \Gamma_g \phi_g \rho_g T_g \frac{d\eta_g}{dt} + \big(c_s^2 - c_g^2\big)\mathcal{C} \, .$$

The time derivatives in $\mathcal{S}$ can be eliminated using the linearly degenerate characteristic equations. Hence $\mathcal{S}$ represents a source term. Linear combinations of Eq. (111) and Eq. (114) yield

$$\Big(\frac{d}{dt} + c\frac{\partial}{\partial x}\Big) P + \rho c \Big(\frac{d}{dt} + c\frac{\partial}{\partial x}\Big) u = \mathcal{S} \tag{115}$$

$$\Big(\frac{d}{dt} - c\frac{\partial}{\partial x}\Big) P - \rho c \Big(\frac{d}{dt} - c\frac{\partial}{\partial x}\Big) u = \mathcal{S} \tag{116}$$

where the average sound speed is given by

$$\rho c^2 = \phi_s \rho_s c_s^2 + \phi_g \rho_g c_g^2 \, . \tag{117}$$

A full set of characteristic equation implies the reduced model is hyperbolic.

B Characteristics for Velocity & Pressure Reduction

The velocity and pressure reduced model consists of the PDEs (66)–(72) plus the pressure equilibrium condition, $P_s = P_g + \beta_s$. Here we express the reduced model in characteristic form. From the derivation of the model it is clear that the three linear degenerate modes associated with the particle trajectory correspond to those in the velocity reduction with the compaction dissipation deleted

$$\phi_s \rho_s T_s \frac{d\eta_s}{dt} = -(T_s - T_g)\mathcal{H} \, , \tag{118}$$

$$\phi_g \rho_g T_g \frac{d\eta_g}{dt} = (T_s - T_g)\mathcal{H} - \big[H_s - H_g - (P_s - P_g - \beta_s)V_s\big]\mathcal{C} \, , \tag{119}$$

$$\frac{d}{dt}\Big(\frac{\phi_s \rho_s}{\rho}\Big) = \frac{\mathcal{C}}{\rho} \, . \tag{120}$$

To derive the acoustic mode we rewrite the mixture momentum balance as

$$\rho \frac{du}{dt} + \frac{\partial P}{\partial x} = 0. \tag{121}$$

Next we derive an equation for the pressure. It follows from the pressure equilibrium condition that

$$\frac{dP}{dt} = \phi_s \frac{dP_s}{dt} + \phi_g \frac{dP_g}{dt} + \beta_s \frac{d\phi_s}{dt} \, .$$

The mass balance equations can again be expressed in terms of the phase pressures, Eqs. (112) and (113). Adding these equation results in

$$\frac{dP}{dt} + \Big(\phi_s\rho_s c_s^2 + \phi_g\rho_g c_g^2\Big)\frac{\partial u}{\partial x} = -\Big(\rho_s c_s^2 - \rho_g c_g^2 - \beta_s\Big)\frac{d\phi_s}{dt} + \Gamma_s\phi_s\rho_s T_s\frac{d\eta_s}{dt} + \Gamma_g\phi_g\rho_g T_g\frac{d\eta_g}{dt} + \big(c_s^2 - c_g^2\big)\mathcal{C}\ .$$

Applying Eq. (72) to eliminate $\frac{d\phi_s}{dt}$ yields

$$\frac{dP}{dt} + \rho\, c_{\rm eq}^2\frac{\partial u}{\partial x} = \mathcal{S}\ , \tag{122}$$

where $c_{\rm eq}$ is given by

$$\rho c_{\rm eq}^2 = \Big(\phi_s\rho_s c_s^2 + \phi_g\rho_g c_g^2\Big) - \frac{\big(\rho_s c_s^2 - \rho_g c_g^2 - \beta_s\big)^2}{\frac{\rho_s c_s^2}{\phi_s} + \frac{\rho_g c_g^2}{\phi_g} + \phi_s\rho_s\frac{d^2B}{d\phi_s^2}}\ , \tag{123}$$

the source $\mathcal{S}$ is given by

$$\mathcal{S} = -\frac{\Big(\rho_s c_s^2 - \rho_g c_g^2 - \beta_s\Big)\Big[\mathcal{B} - \Big(\frac{\Gamma_s}{\phi_s} + \frac{\Gamma_g}{\phi_g}\Big)(T_s - T_g)\mathcal{H}\Big]}{\frac{\rho_s c_s^2}{\phi_s} + \frac{\rho_g c_g^2}{\phi_g} + \phi_s\rho_s\frac{d^2B}{d\phi_s^2}} + \frac{\Gamma_g\rho_g T_g}{c_g^2}\frac{d\eta_g}{dt} + \frac{\Gamma_s\rho_s T_s}{c_s^2}\frac{d\eta_s}{dt} + \big(c_s^2 - c_g^2\big)\mathcal{C}\ , \tag{124}$$

and the extra burn term from the compaction equation is

$$\mathcal{B} = \left[2\frac{c_s^2}{\phi_s} + \left(1 + \frac{\rho_g}{\rho_s}\right)\frac{c_g^2}{\phi_g} + \frac{\Gamma_g}{\phi_g}\Big(H_s - H_g - (P_s - P_g - \beta_s)V_s\Big) - \frac{\beta_s}{\phi_s\rho_s}\right]\mathcal{C}\ .$$

Again the time derivative terms in $\mathcal{S}$ can be eliminated using the linearly degenerate characteristic equations. Linear combinations of Eqs. (121) and (122), yield

$$\Big(\frac{d}{dt} + c_{\rm eq}\frac{\partial}{\partial x}\Big)P + \rho\, c_{\rm eq}\Big(\frac{d}{dt} + c_{\rm eq}\frac{\partial}{\partial x}\Big)u = \mathcal{S}\ , \tag{125}$$

$$\Big(\frac{d}{dt} - c_{\rm eq}\frac{\partial}{\partial x}\Big)P - \rho\, c_{\rm eq}\Big(\frac{d}{dt} - c_{\rm eq}\frac{\partial}{\partial x}\Big)u = \mathcal{S}\ . \tag{126}$$

Physical considerations lead us to assume that $B(\phi_s)$ is convex and $\gamma_s > \gamma_g > 1$. Under these conditions, pressure equilibrium implies that $\rho_s c_s^2 > \rho_g c_g^2 + \beta_s$ and the equilibrium sound speed is bounded by $\tilde{c}_{\rm eq} \le c_{\rm eq} < c$ where c is the average sound speed given by Eq. (117), and $\tilde{c}_{\rm eq}$, obtained by setting $B = 0$ and $\beta_s = 0$, can be expressed as

$$\frac{1}{\rho\,\tilde{c}_{\rm eq}^2} = \frac{\phi_s}{\rho_s c_s^2} + \frac{\phi_g}{\rho_g c_g^2}\ . \tag{127}$$

The expression for $\tilde{c}_{\rm eq}$ is a standard result for equilibrium two-phase fluid flow in the absence of a configuration pressure; see *e.g.*, [37] or [10]. The fact that $c_{\rm eq}^2 > 0$ implies that there are a full set of characteristic equations. Hence, the reduced model is hyperbolic.

C Details of compaction-zone analysis

With the equations of state Eqs. (101) and (102) at hand, the mixture energy takes the form

$$\begin{aligned}\bar{e} = \frac{\phi_s\bar{\rho}_s\bar{e}_s + \phi_g\bar{\rho}_g\bar{e}_g}{\bar{\rho}} \ &= \ \bar{\mathcal{U}}(\phi_s\bar{\rho}_s\bar{e}_s + \phi_g\bar{\rho}_g\bar{e}_g) \\ = \bar{\mathcal{U}}\left\{\frac{\phi_s\bar{P}_s}{(\gamma_s - 1)} + \frac{\phi_g\bar{P}_g}{(\gamma_g - 1)} + \frac{\phi_s}{\gamma_s - 1}\left(\gamma_s\bar{P}_{s0}^* - \frac{\bar{\rho}_s}{\bar{\rho}_{s0}}(\bar{P}_{s0} + \gamma_s\bar{P}_{s0}^*)\right)\right\}&.\end{aligned} \tag{128}$$

Note also that

$$\bar{e}_0 = \frac{\phi_{g0}\bar{P}_{g0}}{\gamma_g - 1}. \tag{129}$$

Now, Eqs. (96) and (97) may be solved for the densities, to yield

$$\bar{\rho}_s = \frac{\phi_{s0}\bar{\rho}_{s0}}{\phi_s\bar{\mathcal{U}}}, \;\; \bar{\rho}_g = \frac{\phi_{g0}\bar{\rho}_{g0}}{\phi_g\bar{\mathcal{U}}}. \tag{130}$$

To solve for the pressures we rewrite Eq. (98) as

$$\phi_s\bar{P}_s + \phi_g\bar{P}_g = \bar{P}_0 - \bar{\mathcal{U}} + 1 \equiv \mathcal{R}_1, \tag{131}$$

and with the aid of Eqs. (128), (129), the first of (130) and (131), we rewrite Eq. (99) as

$$\begin{aligned}\frac{\phi_s\bar{P}_s}{(\gamma_s-1)} + \frac{\phi_g\bar{P}_g}{(\gamma_g-1)} = \frac{\bar{P}_0(1-\bar{\mathcal{U}})}{\bar{\mathcal{U}}} + \frac{(1-\bar{\mathcal{U}}^2)}{2\bar{\mathcal{U}}} - (1-\bar{\mathcal{U}}) \\ + \frac{1}{\bar{\mathcal{U}}}\left(\frac{\phi_{s0}\bar{P}_{s0}}{\gamma_s-1} + \frac{\phi_{g0}\bar{P}_{g0}}{\gamma_g-1}\right) + \frac{\gamma_s\bar{P}^*_{s0}}{\gamma_s-1}\left(\frac{\phi_{s0}}{\bar{\mathcal{U}}} - \phi_s\right).\end{aligned} \tag{132}$$

The last term above can be rearranged as

$$\frac{\gamma_s\bar{P}^*_{s0}}{\gamma_s-1}\left(\frac{\phi_{s0}}{\bar{\mathcal{U}}} - \phi_s\right) = \frac{\gamma_s\bar{P}^*_{s0}}{\gamma_s-1}\left(\phi_{s0}\frac{1-\bar{\mathcal{U}}}{\bar{\mathcal{U}}} - (\phi_s - \phi_{s0})\right),$$

allowing Eq. (132) to take the form

$$\begin{aligned}\frac{\phi_s\bar{P}_s}{(\gamma_s-1)} + \frac{\phi_g\bar{P}_g}{(\gamma_g-1)} = \frac{\bar{P}_0(1-\bar{\mathcal{U}})}{\bar{\mathcal{U}}} + \frac{(1-\bar{\mathcal{U}}^2)}{2\bar{\mathcal{U}}} - (1-\bar{\mathcal{U}}) + \frac{1}{\bar{\mathcal{U}}}\left(\frac{\phi_{s0}\bar{P}_{s0}}{\gamma_s-1} + \frac{\phi_{g0}\bar{P}_{g0}}{\gamma_g-1}\right) \\ + \frac{\gamma_s\bar{P}^*_{s0}}{\gamma_s-1}\left\{\left(\frac{1-\bar{\mathcal{U}}}{\bar{\mathcal{U}}}\right)\phi_{s0} - (\phi_s - \phi_{s0})\right\}.\end{aligned} \tag{133}$$

To achieve further consolidation of the above expression, we define constants γ and γ_1 via the relations

$$\frac{1}{\gamma} = \frac{1}{\gamma_g - 1} - \frac{1}{\gamma_s - 1}, \tag{134}$$

and

$$\frac{1}{\gamma_1} = \frac{\phi_{g0}}{\gamma_g - 1} + \frac{\phi_{s0}}{\gamma_s - 1}. \tag{135}$$

Then, recognizing that $\bar{P}_0 = \bar{P}_{s0} = \bar{P}_{g0}$, Eq. (133) can be written as

$$\begin{aligned}\frac{\phi_s\bar{P}_s}{(\gamma_s-1)} + \frac{\phi_g\bar{P}_g}{(\gamma_g-1)} &= \frac{1-\bar{\mathcal{U}}}{\bar{\mathcal{U}}}\left[\bar{P}_0\left(1+\frac{1}{\gamma_1}\right) + \frac{\gamma_s\bar{P}^*_{s0}\phi_{s0}}{\gamma_s-1} + \frac{1-\bar{\mathcal{U}}}{2}\right] + \frac{\bar{P}_0}{\gamma_1} - \frac{\gamma_s\bar{P}^*_{s0}}{\gamma_s-1}(\phi_s - \phi_{s0}) \\ &= \frac{1-\bar{\mathcal{U}}}{\bar{\mathcal{U}}}\left[\bar{P}_0\left(1+\frac{1}{\gamma_1}\right) + \frac{\gamma_s\bar{P}^*_{s0}\phi_{s0}}{\gamma_s-1} + \tfrac{1}{2} - \bar{\mathcal{U}}\left(\tfrac{1}{2}+\frac{1}{\gamma_1}\right)\right] \\ &\qquad + \frac{\bar{P}_0 + 1 - \bar{\mathcal{U}}}{\gamma_1} - \frac{\gamma_s\bar{P}^*_{s0}}{\gamma_s-1}(\phi_s - \phi_{s0}) \\ &= \left(\tfrac{1}{2}+\frac{1}{\gamma_1}\right)\frac{1-\bar{\mathcal{U}}}{\bar{\mathcal{U}}}(\bar{\mathcal{U}}_2 - \bar{\mathcal{U}}) + \frac{\bar{P}_0 + 1 - \bar{\mathcal{U}}}{\gamma_1} - \frac{\gamma_s\bar{P}^*_{s0}}{\gamma_s-1}(\phi_s - \phi_{s0}) \equiv \mathcal{R}_2,\end{aligned} \tag{136}$$

where we have defined $\bar{\mathcal{U}}_2$ as

$$\bar{\mathcal{U}}_2 \equiv \frac{\bar{P}_0\left(1+\frac{1}{\gamma_1}\right)+\frac{\gamma_s\phi_{s0}\bar{P}^*_{s0}}{\gamma_s-1}+\frac{1}{2}}{\frac{1}{2}+\frac{1}{\gamma_1}}. \tag{137}$$

Now, Eqs. (131) and (136) may be solved simultaneously to yield $\bar{P}_s$ and $\bar{P}_g$ as functions of $\bar{\mathcal{U}}$ and ϕ_s, and we obtain

$$\bar{P}_s = -\frac{\gamma}{\phi_s}\left(\mathcal{R}_2 - \frac{\mathcal{R}_1}{\gamma_g-1}\right), \quad \bar{P}_g = \frac{\gamma}{\phi_g}\left(\mathcal{R}_2 - \frac{\mathcal{R}_1}{\gamma_s-1}\right). \tag{138}$$

One is now able to construct an expression for the pressure difference between the phases, in terms of ϕ_s and $\bar{\mathcal{U}}$, as

$$\bar{P}_s - \bar{P}_g = -\frac{\gamma}{\phi_s\phi_g}\left\{\mathcal{R}_2 - \mathcal{R}_1\left(\frac{\phi_s}{\gamma_s-1}+\frac{\phi_g}{\gamma_g-1}\right)\right\}. \tag{139}$$

Note that in view of Eqs. (134) and (135), the expression within the parentheses on the right can be rewritten as

$$\frac{\phi_s}{\gamma_s-1}+\frac{\phi_g}{\gamma_g-1} = \frac{1}{\gamma_1} - \frac{\phi_s-\phi_{s0}}{\gamma}. \tag{140}$$

The above result, along with the expressions for $\mathcal{R}_1$ and $\mathcal{R}_2$, defined in Eqs. (131) and (136), respectively, allows Eq. (139) to assume the form

$$\bar{P}_s - \bar{P}_g = -\frac{\gamma}{\phi_s\phi_g}\left[\left(\tfrac{1}{2}+\frac{1}{\gamma_1}\right)\frac{1-\bar{\mathcal{U}}}{\bar{\mathcal{U}}}(\bar{\mathcal{U}}_2-\bar{\mathcal{U}}) - \frac{\gamma_s\bar{P}^*_{s0}}{\gamma_s-1}(\phi_s-\phi_{s0}) + \frac{\bar{P}_0+1-\bar{\mathcal{U}}}{\gamma}(\phi_s-\phi_{s0})\right]. \tag{141}$$

We now define $\bar{\mathcal{U}}_1$ by the expression

$$\bar{\mathcal{U}}_1 \equiv 1-\gamma\left(\frac{\gamma_s\bar{P}^*_{s0}}{\gamma_s-1}-\frac{\bar{P}_0}{\gamma}\right), \tag{142}$$

which allows Eq. (141) to be put into the compact form

$$\bar{P}_s - \bar{P}_g = -\frac{\gamma}{\phi_s\phi_g}\left[\left(\tfrac{1}{2}+\frac{1}{\gamma_1}\right)\frac{1-\bar{\mathcal{U}}}{\bar{\mathcal{U}}}(\bar{\mathcal{U}}_2-\bar{\mathcal{U}}) - \frac{\phi_s-\phi_{s0}}{\gamma}(\bar{\mathcal{U}}-\bar{\mathcal{U}}_1)\right]. \tag{143}$$

On setting $\bar{P}_s - \bar{P}_g = 0$, we obtain the pressure-equilibrium locus in the $\phi_s - \bar{\mathcal{U}}$ plane as

$$\frac{\phi_s-\phi_{s0}}{1-\phi_{s0}} = \mathcal{L}_E(\bar{\mathcal{U}}) \equiv \frac{\gamma}{1-\phi_{s0}}\left(\tfrac{1}{2}+\frac{1}{\gamma_1}\right)\frac{(1-\bar{\mathcal{U}})(\bar{\mathcal{U}}_2-\bar{\mathcal{U}})}{\bar{\mathcal{U}}(\bar{\mathcal{U}}-\bar{\mathcal{U}}_1)}, \tag{144}$$

where $\bar{\mathcal{U}}_1$ and $\bar{\mathcal{U}}_2$ are defined by Eqs. (142) and (137), respectively. The state at the end of the compaction wave must lie on this locus.

We now turn to the gas isentrope,

$$\frac{\bar{P}_g}{\bar{P}_{g0}} = \left(\frac{\bar{\rho}_g}{\bar{\rho}_{g0}}\right)^{\gamma_g},$$

and attempt to express it as well as a locus in the ϕ_s,$\bar{\mathcal{U}}$-plane. On substituting for $\bar{\rho}_g$ from the second of expressions in Eq. (130), and for $\bar{P}_g$ from the second of expressions in Eq. (138), we get

$$\bar{P}_{g0}\left\{\frac{\phi_{g0}}{\bar{\mathcal{U}}(1-\phi_s)}\right\}^{\gamma_g} = \frac{\gamma}{1-\phi_s}\left\{\mathcal{R}_2 - \frac{\mathcal{R}_1}{\gamma_s-1}\right\}. \tag{145}$$

Substituting for $\mathcal{R}_1$ and $\mathcal{R}_2$, from Eqs. (131) and (136), respectively, we find that

$$\frac{\bar{P}_{g0}\phi_{g0}}{\gamma\bar{\mathcal{U}}}\left\{\frac{\phi_{g0}}{\bar{\mathcal{U}}(1-\phi_s)}\right\}^{\gamma_g-1} = \left(\tfrac{1}{2}+\frac{1}{\gamma_1}\right)\frac{1-\bar{\mathcal{U}}}{\bar{\mathcal{U}}}(\bar{\mathcal{U}}_2-\bar{\mathcal{U}}) + \frac{\bar{P}_0+1-\bar{\mathcal{U}}}{\gamma_1} - \frac{\bar{P}_0+1-\bar{\mathcal{U}}_1}{\gamma}(\phi_s-\phi_{s0}) - \frac{\bar{P}_0+1-\bar{\mathcal{U}}}{\gamma_s-1}. \quad (146)$$

Recognizing that $\phi_s - \phi_{s0} = \phi_{g0} - \phi_g$ and that

$$\frac{1}{\gamma_1} - \frac{1}{\gamma_s-1} = \frac{\phi_{g0}}{\gamma},$$

Eq. (146) can be rewritten as

$$\frac{\bar{P}_{g0}\phi_{g0}}{\gamma\bar{\mathcal{U}}}\left\{\frac{\phi_{g0}}{\bar{\mathcal{U}}(1-\phi_s)}\right\}^{\gamma_g-1} = \left(\tfrac{1}{2}+\frac{1}{\gamma_1}\right)\frac{1-\bar{\mathcal{U}}}{\bar{\mathcal{U}}}(\bar{\mathcal{U}}_2-\bar{\mathcal{U}}) + \frac{(\bar{\mathcal{U}}_1-\bar{\mathcal{U}})\phi_{g0}}{\gamma} + \frac{\bar{P}_0+1-\bar{\mathcal{U}}_1}{\gamma}\phi_g,$$

or, as

$$\bar{P}_0\left\{\frac{1}{\bar{\mathcal{U}}\left(1-\frac{\phi_s-\phi_{s0}}{1-\phi_{s0}}\right)}\right\}^{\gamma_g-1} = \frac{\gamma}{1-\phi_{s0}}\left(\tfrac{1}{2}+\frac{1}{\gamma_1}\right)(1-\bar{\mathcal{U}})(\bar{\mathcal{U}}_2-\bar{\mathcal{U}}) + (\bar{\mathcal{U}}_1-\bar{\mathcal{U}})\bar{\mathcal{U}} + (\bar{P}_0+1-\bar{\mathcal{U}}_1)\bar{\mathcal{U}}\left(1-\frac{\phi_s-\phi_{s0}}{1-\phi_{s0}}\right).$$

Finally, a slight manipulation leads to the gas isentrope as the implicit locus

$$\mathcal{L}_I(\bar{\mathcal{U}},\phi_s) \equiv (\bar{P}_0+1-\bar{\mathcal{U}}_1)\bar{\mathcal{U}}\frac{\phi_s-\phi_{s0}}{1-\phi_{s0}} + \bar{P}_0\left\{\frac{1}{\bar{\mathcal{U}}\left(1-\frac{\phi_s-\phi_{s0}}{1-\phi_{s0}}\right)}\right\}^{\gamma_g-1} - \frac{\gamma}{1-\phi_{s0}}\left(\tfrac{1}{2}+\frac{1}{\gamma_1}\right)(1-\bar{\mathcal{U}})(\bar{\mathcal{U}}_2-\bar{\mathcal{U}}) - (\bar{P}_0+1-\bar{\mathcal{U}})\bar{\mathcal{U}} \;=\; 0 \quad (147)$$

in the $\phi_s, \bar{\mathcal{U}}$-plane.

Before proceeding further, we note that Eq. (142) for $\bar{\mathcal{U}}_1$ can be put into a more symmetric form. Thus, upon using the definition Eq. (134) for γ, Eq. (142) becomes

$$\begin{aligned}
\bar{\mathcal{U}}_1 &= 1-\gamma\left[\frac{\gamma_s\bar{P}^*_{s0}}{\gamma_s-1} - \bar{P}_0\left(\frac{1}{\gamma_g-1}-\frac{1}{\gamma_s-1}\right)\right] \\
&= 1-\gamma\left[\frac{\gamma_s\bar{P}^*_{s0}}{\gamma_s-1} - \bar{P}_0\left(\frac{\gamma_g}{\gamma_g-1}-\frac{\gamma_s}{\gamma_s-1}\right)\right] \\
&= 1-\gamma\left[\frac{\gamma_s(\bar{P}^*_{s0}+P_{s0})}{\gamma_s-1} - \frac{\gamma_g\bar{P}_{g0}}{\gamma_g-1}\right] \\
&= 1-\gamma\left(\frac{\bar{\rho}_{s0}\bar{c}^2_{s0}}{\gamma_s-1} - \frac{\bar{\rho}_{g0}\bar{c}^2_{g0}}{\gamma_g-1}\right). \qquad (148)
\end{aligned}$$

Similarly, on using the definition Eq. (135) of γ_1, we can rewrite Eq. (137) for $\bar{\mathcal{U}}_2$ as

$$\begin{aligned}\bar{\mathcal{U}}_2 &= \frac{\bar{P}_0\left(1+\frac{\phi_{s0}}{\gamma_s-1}+\frac{\phi_{g0}}{\gamma_g-1}\right)+\frac{\gamma_s\phi_{s0}\bar{P}^*_{s0}}{\gamma_s-1}+\frac{1}{2}}{\frac{1}{2}+\frac{\phi_{s0}}{\gamma_s-1}+\frac{\phi_{g0}}{\gamma_g-1}} \\ &= \frac{\bar{P}_0\left(\frac{\gamma_s\phi_{s0}}{\gamma_s-1}+\frac{\gamma_g\phi_{g0}}{\gamma_g-1}\right)+\frac{\gamma_s\phi_{s0}\bar{P}^*_{s0}}{\gamma_s-1}+\frac{1}{2}}{\frac{1}{2}+\frac{\phi_{s0}}{\gamma_s-1}+\frac{\phi_{g0}}{\gamma_g-1}} \\ &= \frac{\frac{\gamma_s\phi_{s0}(\bar{P}_{s0}+\bar{P}^*_{s0})}{\gamma_s-1}+\frac{\gamma_g\phi_{g0}\bar{P}_{g0}}{\gamma_g-1}+\frac{1}{2}}{\frac{1}{2}+\frac{\phi_{s0}}{\gamma_s-1}+\frac{\phi_{g0}}{\gamma_g-1}} \\ &= \frac{\frac{\phi_{s0}\bar{\rho}_{s0}\bar{c}^2_{s0}}{\gamma_s-1}+\frac{\phi_{g0}\bar{\rho}_{g0}\bar{c}^2_{g0}}{\gamma_g-1}+\frac{1}{2}}{\frac{1}{2}+\frac{\phi_{s0}}{\gamma_s-1}+\frac{\phi_{g0}}{\gamma_g-1}}. \end{aligned} \tag{149}$$

We note that $\bar{\mathcal{U}}_1$ and $\bar{\mathcal{U}}_2$ depend upon the state upstream, and, through the nondimensionalization, upon the wave speed D. Further, $\bar{\mathcal{U}}_2$ is always positive, while $\bar{\mathcal{U}}_1$ may be of either sign. However, for the practical case of a stiff solid, $\bar{\mathcal{U}}_1$ is likely to be negative. Finally, at small values of D (and hence, at higher values of the dimensionless sound speeds), $\bar{\mathcal{U}}_2$ is expected to be large, and in particular, larger than unity.

Recalling that the post compaction state is the intersection of the loci $\mathcal{L}_E$ and $\mathcal{L}_I$, we now examine these loci in some detail. In doing so, we only need concern ourselves with the region $0 \le \bar{\mathcal{U}} \le 1, \quad \phi_{s0} \le \phi_s \le 1$ in the $\phi_s, \bar{\mathcal{U}}$-plane. It is useful to take, as the ordinate, the scaled volume fraction $\phi \equiv (\phi_s - \phi_{s0})/(1-\phi_{s0})$, for which the interval of interest then becomes $[0,1]$. From Eq. (144), the slope of the equilibrium locus at the point $\bar{\mathcal{U}} = 1,\ \phi = 0$ is found to be

$$\mathcal{S}_E = \frac{\gamma}{1-\phi_{s0}}\left(\frac{1}{2}+\frac{1}{\gamma_1}\right)\frac{1-\bar{\mathcal{U}}_2}{1-\bar{\mathcal{U}}_1}. \tag{150}$$

This slope may be positive or negative, depending upon the relative magnitudes of $\bar{\mathcal{U}}_1$ and $\bar{\mathcal{U}}_2$, but is expected to be negative, at least for low wave speeds, in view of the remarks made in the paragraph following Eq. (149).

The gas isentrope, $\mathcal{L}_I$, also originates at the point $(1,0)$ and is, in fact, the actual trajectory of the wave structure in the $\bar{\mathcal{U}}, \phi$-plane. One expects ϕ to increase, and $\bar{\mathcal{U}}$ to decrease, along the trajectory (with the structure terminating at the intersection with the equilibrium locus). As such, one expects the slope of the trajectory at $(1,0)$ to be negative. This slope, as computed from Eq. (147), is given by

$$\mathcal{S}_I = \frac{\gamma_g\bar{P}_0 - 1 + \frac{\gamma}{1-\phi_{s0}}\left(\frac{1}{2}+\frac{1}{\gamma_1}\right)(1-\bar{\mathcal{U}}_2)}{\gamma_g\bar{P}_0 + 1 - \bar{\mathcal{U}}_1}. \tag{151}$$

The minimum admissible wave speed of the compaction wave corresponds to the two loci being just tangent to each other at $(1,0)$. Equating the two slopes computed above, followed by simple algebraic manipulation, we get

$$\frac{\gamma_g\bar{P}_0 - 1}{\gamma_g\bar{P}_0 + 1 - \bar{\mathcal{U}}_1} = \frac{\gamma}{1-\phi_{s0}}\left(\frac{1}{2}+\frac{1}{\gamma_1}\right)(1-\bar{\mathcal{U}}_2)\left(\frac{1}{1-\bar{\mathcal{U}}_1} - \frac{1}{\gamma_g\bar{P}_0 + 1 - \bar{\mathcal{U}}_1}\right),$$

or,

$$(\gamma_g\bar{P}_0 - 1)(1-\bar{\mathcal{U}}_1) = \frac{\gamma}{1-\phi_{s0}}\left(\frac{1}{2}+\frac{1}{\gamma_1}\right)(1-\bar{\mathcal{U}}_2)\gamma_g\bar{P}_0.$$

Equation (137) allows the above equation to be rewritten as

$$\frac{1-\phi_{s0}}{\gamma}(\gamma_g\bar{P}_0-1)(1-\bar{\mathcal{U}}_1)=\gamma_g\bar{P}_0\left[\frac{1}{\gamma_1}-\bar{P}_0\left(1+\frac{1}{\gamma_1}\right)-\frac{\gamma_s\phi_{s0}\bar{P}^*_{s0}}{\gamma_s-1}\right].$$

We now invoke the definition of γ_1, Eq. (135), and Eq. (148) for $\bar{\mathcal{U}}_1$, and proceed to manipulate the above equation as

$$\begin{aligned}(1-\phi_{s0})(\gamma_g\bar{P}_0-1)&\left(\frac{\bar{\rho}_{s0}\bar{c}^2_{s0}}{\gamma_s-1}-\frac{\bar{\rho}_{g0}\bar{c}^2_{g0}}{\gamma_g-1}\right)\\ &=\gamma_g\bar{P}_0\left[\frac{\phi_{g0}}{\gamma_g-1}+\frac{\phi_{s0}}{\gamma_s-1}-\bar{P}_0\left(\frac{\gamma_g\phi_{g0}}{\gamma_g-1}+\frac{\gamma_s\phi_{s0}}{\gamma_s-1}\right)-\frac{\gamma_s\phi_{s0}\bar{P}^*_{s0}}{\gamma_s-1}\right]\\ &=\gamma_g\bar{P}_0\left[\frac{\phi_{g0}}{\gamma_g-1}+\frac{\phi_{s0}}{\gamma_s-1}-\left\{\frac{\gamma_g\phi_{g0}\bar{P}_{g0}}{\gamma_g-1}+\frac{\gamma_s\phi_{s0}(\bar{P}_{s0}+\bar{P}^*_{s0})}{\gamma_s-1}\right\}\right]\\ &=\gamma_g\bar{P}_0\left[\frac{\phi_{g0}}{\gamma_g-1}+\frac{\phi_{s0}}{\gamma_s-1}-\left\{\frac{\phi_{g0}\bar{\rho}_{g0}\bar{c}^2_{g0}}{\gamma_g-1}+\frac{\phi_{s0}\bar{\rho}_{s0}\bar{c}^2_{s0}}{\gamma_s-1}\right\}\right]\end{aligned}$$

or, upon some cancelation, as

$$\begin{aligned}\frac{\phi_{g0}\bar{\rho}_{g0}\bar{c}^2_{g0}}{\gamma_g-1}-\frac{\phi_{g0}\bar{\rho}_{s0}\bar{c}^2_{s0}}{\gamma_s-1}&=\gamma_g\bar{P}_0\left(\frac{\phi_{g0}}{\gamma_g-1}+\frac{\phi_{s0}}{\gamma_s-1}-\frac{\bar{\rho}_{s0}\bar{c}^2_{s0}}{\gamma_s-1}\right)\\ &=\frac{\gamma_g\phi_{g0}\bar{P}_{g0}}{\gamma_g-1}+\gamma_g\bar{P}_0\left(\frac{\phi_{s0}}{\gamma_s-1}-\frac{\bar{\rho}_{s0}\bar{c}^2_{s0}}{\gamma_s-1}\right).\end{aligned}$$

The first terms on each side cancel as well, and we are left with

$$\gamma_g\bar{P}_0\phi_{s0}-\gamma_g\bar{P}_0\rho_{s0}\bar{c}^2_{s0}+\phi_{g0}\bar{\rho}_{s0}\bar{c}^2_{s0}=0,$$

which can be expressed as

$$\frac{\phi_{s0}}{\bar{\rho}_{s0}\bar{c}^2_{s0}}+\frac{\phi_{g0}}{\bar{\rho}_{g0}\bar{c}^2_{g0}}=1, \tag{152}$$

where we have replaced $\gamma_g\bar{P}_0$ by $\bar{\rho}_{g0}\bar{c}^2_{g0}$. In dimensional terms, the above equation reads

$$\frac{\phi_{s0}}{\rho_{s0}c^2_{s0}}+\frac{\phi_{g0}}{\rho_{g0}c^2_{g0}}=\frac{1}{\rho_0 D^2_{\min}}, \tag{153}$$

where $D_{\min}$ denotes the minimum wave speed for which a compaction wave structure is feasible. The above expression, in fact, identifies $D_{\min}$ as the *equilibrium* sound speed $c_{\mathrm{eq}0}$ of the mixture at the state upstream.

As the compaction wave speed D is increased, the slope $\mathcal{S}_{\mathcal{I}}$ of the isentrope at the upstream state $(1,0)$ in the $\bar{\mathcal{U}},\phi$-plane becomes less negative, and eventually approaches zero. The critical wave speed is obtained by setting $\mathcal{S}_{\mathcal{I}}=0$. Then, Eq. (151) yields

$$\gamma_g\bar{P}_0-1+\frac{\gamma}{1-\phi_{s0}}\left(\tfrac{1}{2}+\frac{1}{\gamma_1}\right)(1-\bar{\mathcal{U}}_2)=0.$$

On substituting for $\bar{\mathcal{U}}_2$ from Eq. (137), the above reduces to

$$\frac{\phi_{g0}(\gamma_g\bar{P}_0-1)}{\gamma}=\bar{P}_0\left(1+\frac{1}{\gamma_1}\right)-\frac{1}{\gamma_1}+\frac{\gamma_s\phi_{s0}\bar{P}^*_{s0}}{\gamma_s-1}.$$

Upon using the definitions of γ and γ_1, we get

$$\gamma_g \phi_{g0} \bar{P}_0 \left(\frac{1}{\gamma_g - 1} - \frac{1}{\gamma_s - 1} \right) = \bar{P}_0 \left(\frac{\gamma_g \phi_{g0}}{\gamma_g - 1} + \frac{\gamma_s \phi_{s0}}{\gamma_s - 1} \right) - \frac{1}{\gamma_s - 1} + \frac{\gamma_s \phi_{s0} \bar{P}^*_{s0}}{\gamma_s - 1}.$$

Cancelation simplifies the above to

$$\gamma_g \phi_{g0} \bar{P}_0 + \gamma_s \phi_{s0} (\bar{P}_0 + \bar{P}^*_{s0}) = 1,$$

or, to

$$\phi_{g0} \bar{\rho}_{g0} \bar{c}^2_{g0} + \phi_{s0} \bar{\rho}_{s0} \bar{c}^2_{s0} = 1. \tag{154}$$

The dimensional version of this equation reads

$$\phi_{g0} \rho_{g0} c^2_{g0} + \phi_{s0} \rho_{s0} c^2_{s0} = \rho_0 D^2_{\rm crit}, \tag{155}$$

where $D_{\rm crit}$ is the maximum speed consistent with the compaction wave structure under study. Let us recall that $D_{\rm crit}$ is also the *frozen* sound speed at the state ahead of the compaction wave. Let us recall further that this is also the *minimum* wave speed at which a velocity discontinuity will travel.

References

[1] M. R. Baer and J. W. Nunziato. A two-phase mixture theory for the deflagration-to-detonation transition in reactive granular materials. *Int. J. Multiphase Flow*, 12:861–889, 1986.

[2] P. Barry Butler and Herman Krier. Analysis of deflagration to detonation transition in high-energy solid propellants. *Combstion and Flame*, 63:31–48, 1986.

[3] P. Barry Butler. Ph.d. thesis. Technical report, University of Illinois, Urbana, Illinois, 1984.

[4] S. S. Gokhale and H. Krier. Modeling of unsteady two-phase reactive flow in porous beds of propellant. *Prog. Energy Combust. Sci.*, 8:1–39, 1982.

[5] J. M. Powers, D. S. Stewart, and H. K. Krier. Theory of two-phase detonation-part I: structure. *Combustion and Flame*, 80(3):280–303, 1990.

[6] J. M. Powers, D. S. Stewart, and H. K. Krier. Theory of two-phase detonation-part II: modeling. *Combustion and Flame*, 80(3):264–279, 1990.

[7] J. B. Bdzil, R. Menikoff, S. F. Son, A. K. Kapila, and D. S. Stewart. Two-phase modelling of DDT in granular materials: A critical examination of modeling issues. *Phys. Fluids*, 11:378–402, 1999.

[8] J. Massoni, R. Saurel, G. Baudin, and G. Demol. A mechanistic model for shock initiation of solid explosives. *Phys. Fluids*, 11:710–735, 1999.

[9] R. Saurel and R. Abgrall. A multiphase godunov method for compressible multifluid and multiphase flows. *J. Comput. Phys.*, 150:425–467, 1999.

[10] H. B. Stewart and B. Wendroff. Two-phase flow: Models and methods. *J. Comput. Phys.*, 56:363–409, 1984.

[11] D. A. Drew and S. L. Passman. *Theory of Multicomponent Fluids*. Springer, 1998.

[12] Gui-Qiang Chen, C. D. Levermore, and Tai-Ping Liu. Hyperbolic conservation-laws with stiff relaxation terms and entropy. *Communications on Pure and Applied Mathematics*, 47:787–830, 1994.

[13] A. K. Kapila, S. F. Son, J. B. Bdzil, R. Menikoff, and D. S. Stewart. Two-phase modelling of DDT: Structure of the velocity-relaxation zone. *Phys. Fluids*, 9[12]:3885–3897, 1997.

[14] S. F. Son, J. B. Bdzil, R. Menikoff, A. K. Kapila, and D. S. Stewart. Two-phase modelling of DDT: Reduced models and numerical simulations. *in preparation*, 1999.

[15] M. R. Baer and J. W. Nunziato. Compressive combustion of granular materials induced by low-velocity impact. In *Ninth Symposium on Detonation*, pages 293–305, 1989.

[16] J. B. Bdzil and S. F. Son. Engineering models of DDT. Technical Report LA-12794-MS, Los Alamos National Lab., 1995.

[17] K. A. Gonthier, R. Menikoff, S. F. Son, and B. W Asay. Modeling compaction-induced energy dissipation of granular hmx. In *Eleventh (International) Symposium on Detonation, Snowmass, CO, Aug. 31, 1998*, 1998.

[18] P. Embid and M. Baer. Mathematical analysis of a two-phase model for reactive granular materials. *Continuum Mech. Thermodyn.*, 4:279–312, 1992.

[19] H. W. Sandusky and R. R. Bernecker. Compressive reaction in porous beds of energetic materials. In *Eighth International Symposium on Detonation*, pages 881–891, 1985.

[20] J. M. McAfee, B. Asay, W. Campbell, and J. B. Ramsay. Deflagration to detonation in granular HMX. In *Ninth (International) Symposium on Detonation, Portland, OR, Aug. 28, 1989*, pages 265–279, 1989.

[21] J. E. Shepherd and D. R. Begeal. Transient compressible flow in porous materials. Technical Report SAND83-1788, Sandia National Lab., 1988.

[22] B. W Asay, S. F. Son, and J. B. Bdzil. An examination of the role of gas permeation during convective burning of granular explosives. *Int. J. Multiphase Flow*, 22:923–952, 1996.

[23] S. A. Sheffield, R. L. Gustavsen, and R. R. Alcon. Shock initiation studies of low density HMX using electromagnetic particle velocity and pvdf stress gauges. In *Tenth (International) Symposium on Detonation, Boston, MA*, 1993.

[24] E. Kober, J. B. Bdzil, and S. F. Son. Modeling DDT in granular explosives with a multidimensional hydrocode. In *APS Topical Conference of Shock Compression in Condensed Matter–1995, Proceedings of the American Physical Society Topical Conference, Seattle, WA*, pages 437–441, 1996.

[25] D. S. Stewart, B. W. Asay, and K. Prasad. Simplified modeling of transition to detonation in porous energetic materials. *Phys. Fluids*, 6:2515–2534, 1994.

[26] S. F. Son, B. W. Asay, and J. B. Bdzil. Inert plug formation in the DDT of granular energetic materials. In *APS Topical Conference of Shock Compression in Condensed Matter–1995, Proceedings of the American Physical Society Topical Conference, Seattle, WA*, pages 441–444, 1996.

[27] Gui-Qiang Chen and Tai-Ping Liu. Zero relaxation and dissipation limits for hyperbolic conservation laws. *Communications on Pure and Applied Mathematics*, 46:755–781, 1993.

[28] L. F. Henderson and R. Menikoff. Triple-shock entropy theorem and its consequences. *J. Fluid Mech.*, 366:179–210, 1998.

[29] R. Menikoff and E. Kober. Equation of state and Hugoniot locus for porous materials: P–α model revisited. In *APS Topical Conference of Shock Compression in Condensed Matter–1999*, (to be published). Also available on the web at, `http://t14web.lanl.gov/Staff/rsm/Papers/DDT/Porous.pdf`.

[30] W. Herrmann. Constitutive equation for the dynamic compaction of ductile porous material. *J. Applied Phys.*, 40:2490–2499, 1969.

[31] M. Carroll and A. C. Holt. Suggested modification of the P–α model for porous materials. *J. Applied Phys.*, 43:759–761, 1972.

[32] Shi Jin and Zhouping Xin. The relaxing schemes for systems of conservation laws in arbitrary space dimensions. *Communications on Pure and Applied Mathematics*, 48:235–276, 1995.

[33] R. Menikoff and E. Kober. Compaction waves in granular HMX. Technical Report LA-13546-MS, Los Alamos National Lab., 1999. Also available on the web at, `http://t14web.lanl.gov/Staff/rsm/Papers/CompactWave/CompactWave.pdf`.

[34] L. Sainsaulieu. Traveling waves solution of convection-diffusion systems whose convection terms are weakly nonconservative: Application to the modeling of two-phase fluid flows. *SIAM J. Appl. Math.*, 55:1552–1576, 1995.

[35] P. Colella, H. M. Glaz, and R. E. Ferguson. Multi-fluid algorithms for Eulerian finite difference methods. *Draft preprint*, Nov. 1993.

[36] D. J. Benson. A mixture theory for contact in multi-material Eulerian formulations. *Computer Methods in Applied Mechanics and Engineering*, 140:59–86, 1997.

[37] G. B. Wallis. *One-Dimensional Two-Phase Flow*. McGraw-Hill, 1969.